A Fast Computation Method of Bands and Band Field Solutions of 3D Periodic Structures Using Broadband Green's Function-Multiple Scattering Theory

Leung Tsang[1], Tien-Hao Liao[2, *], and Shurun Tan[3, 4, 5]

Abstract—We extended the previous 2D method of BBGF-MST (Broadband Green's function-Multiple Scattering Theory) approach to 3D problems in periodic structures. Band Structures and Band Field Solutions are calculated. A feature of BBGF is that the lattice Green's functions are broadband so that the coefficients of the spherical wave expansions are calculated rapidly for many frequencies. These are then used for speedy calculations of the matrix elements of the KKR (Korringa-Kohn-Rostoker) eigenvalue equation. Using BBGF-MST, a low order matrix eigenvalue equation for the bands is derived. For the first two bands, the dimension of the KKR matrix equation is only 4 by 4. With the use of BBGF, the CPU requirement for the BBGF-MST technique is 0.27 seconds on a standard laptop for solving the KKR eigenvalue equation. Numerical results of the band diagrams are illustrated. Higher order spherical waves are next used to calculate the normalized band field solutions for the entire cell.

1. INTRODUCTION

The calculations of band diagrams and band field solutions are of current interests for applications to photonic crystals, topological photonics and topological acoustics [1–8]. The advantage of the plane wave expansion method for such calculations [9–12] is that the eigenvalue problem is a linear eigenvalue problem. The disadvantage of the method is the poor convergence of the plane waves requiring a large number of plane waves. It requires many plane waves to achieve convergence particularly for large contrasts between the scatterer and the background host materials. Discrete methods such as the finite element method (FEM) [13, 14] and the finite difference method (FDM) [6] have been used. The commercial software COMSOL, which is based on FEM, has also been used by researchers. A common advantage of FEM and FDM is that the Bloch boundary conditions can be readily imposed on the cell boundary of the (0, 0, 0) reference cell so that the FEM or the FDM required solution is reduced to the single (0, 0, 0) cell. The disadvantages of the FDM and FEM methods are that volumetric discretization of the unit cell is required. It requires large number of elements for volumetric discretization, particularly for 3D problems, giving an eigenvalue problem of relatively large matrix dimension in FEM and FDM.

Recently we developed Broadband Green's functions (BBGF) method [7, 8, 15–18] for band diagram calculations with two distinct features. Firstly, after an initial setup is completed, the calculations for many frequencies are performed rapidly, making the method broadband. Secondly, unlike classical expansions of Green's functions which are poorly convergent, the BBGF expansions are rapidly

convergent by making use of imaginary wavenumber extractions [19–21]. We have implemented BBGF for band calculations in two methods. In the first method, the solutions were obtained by combining the BBGF with the integral equation as solved by the method of moment (MoM). The method is labelled the BBGF-MoM method [7, 15, 16]. More recently, we proposed the second method [8, 17, 18] in which we combined the Broadband Green's function (BBGF) method with the KKR (Korringa-Kohn-Rostoker) method [22, 23] and the Multiple Scattering Theory (MST). We label the method as BBGF-MST. In the usual KKR method [24–28], the convergence of the lattice Green's function is accelerated by the Ewald method which is a single frequency method. Single frequency method of accelerated convergence is not efficient since the search for eigenvalues is required for the nonlinear eigenvalue problem and that calculations of the matrix elements are required for many frequencies. The KKR method has been used for decades. In 1960s, Kambe studied the periodical problem using spherical expansion and derived the connection with multiple scattering [29–31]. In the past, the numerical solution of the KKR is based on lattice Green's function computed with the Ewald's method. However, in the recent decade, the Finite element method (FEM) has become attractive because of the easiness of introducing the Bloch condition on opposite sides of the center (0, 0, 0) cell. Thus, the commercial software COMSOL has become the state of the art. Numerous researchers have used COMSOL. A weakness of the traditional KKR is that the Ewald method is a single frequency method so that computation is not efficient as one has to compute the KKR for many frequencies in order to search the eigenvalues. We have developed the Broadband Green's function (BBGF) which accelerates the computation over frequencies. As shown in our papers, the computation of 1000 frequencies is slightly more than that of just one frequency. In papers 2 and 3, we have shown that using BBGF-MST, our method is at least 2 orders of magnitude faster than COMSOL. In this paper we have extended the BBGF-MST method for scalar 3D. We show the method of fast broadband calculations of lattice Green's functions and the broadband coefficients of $\tilde{D}_{nm}(k, \bar{k}_i)$ for the scalar 3D case.

In BBGF, we use the Broadband Green's function to derive analytic expressions of the broadband transformation to cylindrical waves [8, 17, 18]. The method requires a setup after which the determinant for many frequencies is computed readily. For broadband calculations, the BBGF method is much faster than the Ewald method [19–21]. Other numerical methods include hybrid finite element method-boundary element method (FEM-BEM) [32]. However, if the calculation is one frequency at a time, it will be slow for broadband usage. This is unlike BBGF which is for broadband simulations of the KKR equation.

In the formulation, we utilize the MST in which the band eigenvalue problem is expressed in terms of the single scatterer T matrix of the scatterer. The size of the matrix of the KKR eigenvalue equation is made small because in deriving the matrix equation, the exciting fields are in the extinction region of the scatterer so that low order cylindrical waves can be used. After the eigenvalues are solved, the field throughout the entire cell are calculated by higher order cylindrical waves. We have previously developed the BBGF-MST method to two-dimensional (2D) topological photonics and 2D topological acoustics. It was shown that for the case of 2D problem the BBGF-MST method is many times faster than COMSOL [8, 18, 19].

The previous papers of BBGF-MST were for 2D problems [8, 18, 19]. In this paper, we extend BBGF-MST to three-dimensional (3D) problem of scalar waves with scatterers embedded in a 3D lattice. Three dimensional problems in photonic crystals are much more computation intensive than 2D problems. The size of unit cell is about 0.5 wavelength to 1 wavelength in photonic crystal for the first few bands. The embedded scatterers have high permittivity. To solve the 3D problem, the plane wave expansion method requires many plane waves. Many tetrahedral elements are required in 3D FEM and many points of discretization are required in 3D FDM. In this paper, we use BBGF to derive broadband expressions of the coefficients of spherical waves for the 3D lattice Green's functions. Imaginary extractions are used so that spherical wave coefficients are rapidly convergent. The spherical wave coefficients are then used for speedy calculation of the matrix of the KKR (Korringa-Kohn-Rostoker) eigenvalue equation. In the example in this paper, for the first two bands, the dimension of the KKR matrix equation is only 4 by 4. The low order matrix makes the CPU time as small as 0.27 seconds on a standard laptop for the 3D periodic structure problem. After the eigenvalue is calculated, higher order spherical waves are next used to calculate the normalized band field solutions for the entire cell. Numerical results of the band diagrams are also illustrated. For 2D band problems, all methods such

as FEM, FD, COMSOL, plane waves, and KKR methods are sufficiently fast so that solutions can be obtained in relatively modest CPU. However, 3D band problems are much more computationally intensive. Thus, it is important that in this paper using BBGF-MST, the band eigenvalues of 3D problems require CPU of only 0.27 second using standard laptop.

The organization of this paper is as follows. In Section 2, we describe the BBGF in spherical wave expansions with broad band coefficients calculated with imaginary extractions. In Section 3, we describe the integral equations of exciting field and scattered field in Multiple Scattering Theory. In Section 4, using the spherical wave coefficients and the integral equations, we derive the KKR eigenvalue equation. In Section 5, we use the T matrix of an isolated scatterer in the KKR equation. In Section 6, using the eigenvalue determined, we calculate the coefficients of the higher order spherical waves. In Section 7, we derive the normalization of the bandfield solutions. We illustrate numerical results and the CPU requirements in Section 8. Section 9 is the conclusion.

2. BBGF 3D IN SPHERICAL WAVE EXPANSIONS WITH IMAGINARY EXTRACTIONS

Consider a 3D periodic structure in Figure 1. Let the lattice vector be given by

$$\bar{R}_{mnl} = m\bar{a}_1 + n\bar{a}_2 + l\bar{a}_3; \quad m, n, l = 0, \pm 1, \dots \tag{1}$$

where $\bar{a}_1$, $\bar{a}_2$ and $\bar{a}_3$ are the primitive translation vectors. Then $\Omega_0 = \bar{a}_1 \times \bar{a}_2 \cdot \bar{a}_3$ is the size of the cell. The region occupied by the (m, n, l) cell is denoted by Ω_{mnl}. The extent of the $(0, 0, 0)$ cell are $-\frac{\bar{a}_1}{2}$ to $\frac{\bar{a}_1}{2}$ in $\bar{a}_1$ direction, $-\frac{\bar{a}_2}{2}$ to $\frac{\bar{a}_2}{2}$ in $\bar{a}_2$ direction, and $-\frac{\bar{a}_3}{2}$ to $\frac{\bar{a}_3}{2}$ in $\bar{a}_3$ direction.
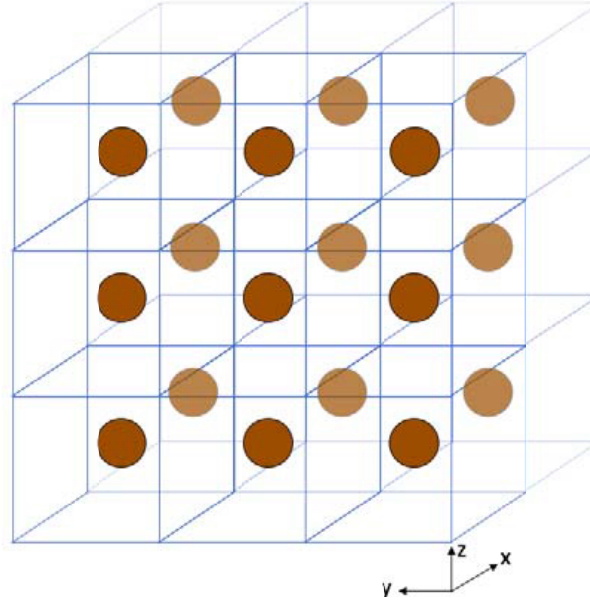
Figure 1. 3D simple cubic (SC) lattice.

The reciprocal lattice vectors are

$$\bar{G}_{mnl} = m\bar{b}_1 + n\bar{b}_2 + l\bar{b}_3; \quad m, n, l = 0, \pm 1, \dots \tag{2}$$

where

$$\bar{b}_1 = 2\pi \frac{\bar{a}_2 \times \bar{a}_3}{\Omega_0}; \quad \bar{b}_2 = 2\pi \frac{\bar{a}_3 \times \bar{a}_1}{\Omega_0}; \quad \bar{b}_3 = 2\pi \frac{\bar{a}_1 \times \bar{a}_2}{\Omega_0} \tag{3}$$

Let $\bar{k}_i$ be a wave vector in the first Brillouin zone

$$\bar{k}_i = \beta_1 \bar{b}_1 + \beta_2 \bar{b}_2 + \beta_3 \bar{b}_3; \quad -\frac{1}{2} \leq \beta_1, \beta_2, \beta_3 \leq \frac{1}{2} \tag{4}$$

Let

$$\bar{k}_{imnl} = \bar{k}_i + \bar{G}_{mnl} \tag{5}$$

be the Bloch vector in the (m, n, l) Brillouin zone. To abbreviate, we replace (m, n, l) by a single index s, so that $(m, n, l) \to s$ and $\sum_s = \sum_{m,n,l}$. The lattice Green's function can be written in spectral form and in spatial form. In spectral form

$$g_P\left(k, \bar{k}_i, \bar{r}\right) = \frac{1}{\Omega_0} \sum_s \frac{e^{i\bar{k}_{is}\cdot\bar{r}}}{k_{is}^2 - k^2} \tag{6}$$

with $k_{is} = |\bar{k}_{imnl}| = |\bar{k}_{is}|$.

Let

$$g_0\left(k, r\right) = \frac{e^{ikr}}{4\pi r} \tag{7}$$

be the free space Green's function. The lattice Green's function in spatial form is

$$g_P\left(k, \bar{k}_i, \bar{r}\right) = \sum_s g_0\left(k, |\bar{r} - \bar{R}_s|\right) e^{i\bar{k}_i\cdot\bar{R}_s} = \sum_s \frac{e^{ik|\bar{r}-\bar{R}_s|}}{4\pi |\bar{r} - \bar{R}_s|} e^{i\bar{k}_i\cdot\bar{R}_s} \tag{8}$$

BBGF consists of broadband calculations of periodic Green's functions for many wavenumbers k or frequencies with accelerated convergence using imaginary extractions. BBGF with 8th order convergence is

$$g_P\left(k, \bar{k}_i, \bar{r}\right) = g_P\left(i\xi, \bar{k}_i, \bar{r}\right) - \frac{\xi^2 + k^2}{2\xi}\left(\frac{d}{d\xi}\right) g_P\left(i\xi, \bar{k}_i, \bar{r}\right) + \frac{\left(\xi^2 + k^2\right)^2}{8\xi}\left(\frac{d}{d\xi}\frac{1}{\xi}\frac{d}{d\xi}\right) g_P\left(i\xi, \bar{k}_i, \bar{r}\right)$$
$$+ \frac{\left(\xi^2 + k^2\right)^3}{\Omega_0} \sum_s e^{i\bar{k}_{is}\cdot\bar{r}} \left[\frac{1}{\left(k_{is}^2 + \xi^2\right)^3 \left(k_{is}^2 - k^2\right)}\right] \tag{9}$$

where $g_P(i\xi, \bar{k}_i, \bar{r})$ is represented in spatial form

$$g_P\left(i\xi, \bar{k}_i, \bar{r}\right) = \sum_s \frac{e^{-\xi|\bar{r}-\bar{R}_s|}}{4\pi |\bar{r} - \bar{R}_s|} e^{i\bar{k}_i\cdot\bar{R}_s} \tag{10}$$

Then

$$\left(\frac{d}{d\xi}\right) g_P\left(i\xi, \bar{k}_i, \bar{r}\right) = \sum_s (-|\bar{r} - \bar{R}_s|) \frac{e^{-\xi|\bar{r}-\bar{R}_s|}}{4\pi |\bar{r} - \bar{R}_s|} e^{i\bar{k}_i\cdot\bar{R}_s} \tag{11}$$

$$\left(\frac{d^2}{d\xi^2}\right) g_P\left(i\xi, \bar{k}_i, \bar{r}\right) = \sum_s |\bar{r} - \bar{R}_s|^2 \frac{e^{-\xi|\bar{r}-\bar{R}_s|}}{4\pi |\bar{r} - \bar{R}_s|} e^{i\bar{k}_i\cdot\bar{R}_s} \tag{12}$$

and

$$\left(\frac{d}{d\xi}\left(\frac{1}{\xi}\frac{d}{d\xi}\right)\right) g_P\left(i\xi, \bar{k}_i, \bar{r}\right) = -\frac{1}{\xi^2}\left(\frac{d}{d\xi}\right) g_P\left(i\xi, \bar{k}_i, \bar{r}\right) + \frac{1}{\xi}\left(\frac{d^2}{d\xi^2}\right) g_P\left(i\xi, \bar{k}_i, \bar{r}\right) \tag{13}$$

In Equation (9), the spatial expansion series in the first 3 terms are independent of wave numbers and are fast exponentially convergent with $\bar{R}_s$ because of the use of imaginary wave number $i\xi$.

The spectral expansion series in the 4th term in Equation (9) has an 8th order convergence because of the asymptotic k_{is}^{-8} dependence. The 4th term is broadband because the dependence on k is merely $(\xi^2 + k^2)^3(k_{is}^2 - k^2)^{-1}$ with the rest of the expression being independent of k.

We shall illustrate in the numerical results section, the band field solutions in the unit cell are well represented by spherical waves. We then seek solutions of the band fields in terms of spherical waves. Let (r, θ, ϕ) denote spherical coordinates. The spherical wave functions for scalar waves are

$$Rg\psi_{nm}\left(k\bar{r}\right) = j_n\left(kr\right) Y_n^{(N)m}\left(\theta, \phi\right); \quad m = 0, \pm 1, ..., \pm n \tag{14}$$

$$\psi_{nm}\left(kr\right) = h_n^{(1)}\left(kr\right) Y_n^{(N)m}\left(\theta, \phi\right) = \left(j_n\left(kr\right) + in_n(kr)\right) Y_n^{(N)m}\left(\theta, \phi\right); \quad m = 0, \pm 1, ..., \pm n \tag{15}$$

where $Y_n^{(N)m}(\theta,\phi)$ are spherical harmonics, with (N) denoting normalized as defined in Appendix A, $j_n(kr)$, $n_n(kr)$ and $h_n^{(1)}(kr)$ are respectively the spherical Bessel function, the spherical Neuman function and the spherical Hankel function of first kind, all of order n. Rg in Equation (14) stands for "regular" indicating j_n is used. Otherwise, without specifying Rg, $h_n^{(1)}$ will be used. The spherical harmonics defined are different from Tsang et al. Vol. 1 [33]. The lattice Green's functions are expanded in terms of spherical waves with coefficients $\tilde{D}_{nm}(k,\bar{k}_i)$

$$g_P\left(k,\bar{k}_i,\bar{r}\right) = \frac{ik}{\sqrt{4\pi}}\,\psi_{00}(kr) + \frac{ik}{\sqrt{4\pi}}\sum_{nm}\tilde{D}_{nm}\left(k,\bar{k}_i\right)Rg\psi_{nm}\left(k\bar{r}\right) \tag{16}$$

We next derive broadband expressions for the coefficients $\tilde{D}_{nm}(k,\bar{k}_i)$ so that they can be computed fast for many wavenumbers k.

Consider a spherical surface with radius R, where the spherical surface is inside cell $(0, 0, 0)$. Let the $\bar{r}$ in Equation (16) be (R,θ,ϕ). Multiply Equation (16) by complex conjugate $(Y_{n'}^{(N)m'}(\theta,\phi))^*$ and integrate over $\int_0^\pi d\theta\sin\theta\int_0^{2\pi}d\phi$. Use orthonormal relation of spherical harmonics (Appendix A). Then

$$\tilde{D}_{nm}\left(k,\bar{k}_i\right) = \frac{1}{\frac{ik}{\sqrt{4\pi}}j_n(kR)}\left\{\frac{k}{\sqrt{4\pi}}\,n_0(kR)\,\delta_{m0}\delta_{n0}\right.$$
$$\left. + \int_0^\pi d\theta\sin\theta\int_0^{2\pi}d\phi g_P\left(k,\bar{k}_i,|\bar{r}|=R\right)\left(Y_n^{(N)m}(\theta,\phi)\right)^*\right\} - \delta_{m0}\delta_{n0} \tag{17}$$

where $n_0(kR)$ is the spherical Neumann function of order 0. Substitute the 8th order Green's function of Equation (9) in Equation (17), we obtain

$$\tilde{D}_{nm}\left(k,\bar{k}_i\right) = -\frac{h_0^{(1)}(kR)}{j_0(kR)}\delta_{n0}\delta_{m0} + \frac{\sqrt{4\pi}}{ikj_n(kR)}I_1\left(n,m,i\xi,\bar{k}_i\right) - \frac{\sqrt{4\pi}}{ikj_n(kR)}\frac{\xi^2+k^2}{2\xi}I_2(n,m,i\xi,\bar{k}_i)$$
$$+\frac{\sqrt{4\pi}}{ikj_n(kR)}\frac{\left(\xi^2+k^2\right)^2}{8\xi}I_3\left(n,m,i\xi,\bar{k}_i\right)$$
$$+\frac{\sqrt{4\pi}}{ikj_n(kR)}\frac{\left(\xi^2+k^2\right)^3}{\Omega_0}\sum_s I_4\left(n,m,i\xi,\bar{k}_i\right)\left[\frac{1}{\left(k_{is}^2+\xi^2\right)^3\left(k_{is}^2-k^2\right)}\right] \tag{18}$$

where

$$I_1\left(n,m,i\xi,\bar{k}_i\right) = \int_0^\pi d\theta\sin\theta\int_0^{2\pi}d\phi\left(Y_n^{(N)m}(\theta,\phi)\right)^*g_P\left(i\xi,\bar{k}_i,\bar{r}\right) \tag{19}$$

$$I_2\left(n,m,i\xi,\bar{k}_i\right) = \int_0^\pi d\theta\sin\theta\int_0^{2\pi}d\phi\left(Y_n^{(N)m}(\theta,\phi)\right)^*\left(\frac{d}{d\xi}\right)g_P\left(i\xi,\bar{k}_i,\bar{r}\right)$$
$$= \left(\frac{d}{d\xi}\right)I_1\left(n,m,i\xi,\bar{k}_i\right) \tag{20}$$

$$I_3\left(n,m,i\xi,\bar{k}_i\right) = \int_0^\pi d\theta\sin\theta\int_0^{2\pi}d\phi\left(Y_n^{(N)m}(\theta,\phi)\right)^*\left(\frac{d}{d\xi}\left(\frac{1}{\xi}\frac{d}{d\xi}\right)\right)g_P\left(i\xi,\bar{k}_i,\bar{r}\right)$$
$$= \frac{1}{\xi}\frac{d}{d\xi}I_2\left(n,m,i\xi,\bar{k}_i\right) - \frac{1}{\xi^2}I_2\left(n,m,i\xi,\bar{k}_i\right) \tag{21}$$

$$I_4\left(n,m,i\xi,\bar{k}_i\right) = \int_0^\pi d\theta\sin\theta\int_0^{2\pi}d\phi\left(Y_n^{(N)m}(\theta,\phi)\right)^*e^{i\bar{k}_{is}\cdot\bar{r}} \tag{22}$$

The 2-dimensional integrals $\int_0^\pi d\theta\sin\theta\int_0^{2\pi}d\phi$ can be evaluated analytically. In spatial domain, we abbreviate $\sum_{m,n,l}\to\sum_s$. Let $s=0$ term denote the $(0,0,0)$ cell. Since $\bar{r}$ is inside the $(0,0,0)$ cell, we

have, for other cells with $s \neq 0$, $R_s = \left|\bar{R}_s\right| > r$. We decompose $\sum_s = \text{term}_{s=0} + \sum_{s \neq 0}$ term. Then

$$g_P\left(i\xi, \bar{k}_i, \bar{r}\right) = \frac{(-\xi)}{\sqrt{4\pi}} h_0^{(1)}\left(i\xi r\right) \frac{1}{\sqrt{4\pi}} + \sum_{s \neq 0} \frac{(-\xi)}{\sqrt{4\pi}} h_0^{(1)}\left(i\xi \left|\bar{r} - \bar{R}_s\right|\right) \frac{1}{\sqrt{4\pi}} e^{i\bar{k}_i \cdot \bar{R}_s} \tag{23}$$

For $s \neq 0$, let $\bar{R}_s = (R_s, \theta_{R_s}, \phi_{R_s})$ in spherical coordinates. Using addition theorem replace $h_0^{(1)}\left(-\xi \left|\bar{r} - \bar{R}_s\right|\right) \frac{1}{\sqrt{4\pi}}$, with $R_s > r$ for the second term in Equation (23), we have

$$g_P\left(i\xi, \bar{k}_i, \bar{r}\right) = \frac{(-\xi)}{\sqrt{4\pi}} h_0^{(1)}\left(i\xi r\right) \frac{1}{\sqrt{4\pi}} + \sum_{s \neq 0} \frac{(-\xi)}{\sqrt{4\pi}} e^{i\bar{k}_i \cdot \bar{R}_s} \sqrt{4\pi}$$

$$\left[\sum_{n',m'} (-1)^{m'} h_{n'}\left(i\xi R_s\right) Y_{n'}^{(N)m'}\left(\theta_{R_s}, \phi_{R_s}\right) j_{n'}\left(i\xi r\right) Y_{n'}^{(N)(-m')}\left(\theta, \phi\right)\right] \tag{24}$$

Substituting in the integral and using orthonormality of spherical harmonics, we obtain

$$I_1\left(n, m, i\xi, \bar{k}_i\right) = \frac{1}{\sqrt{4\pi}} \frac{e^{-\xi R}}{R} \delta_{n0}\delta_{m0} - \xi j_n\left(i\xi R\right)$$

$$\sum_{s \neq 0} e^{i\bar{k}_i \cdot \bar{R}_s} (-1)^{(m)} h_n\left(i\xi R_s\right) Y_n^{(N)(-m)}\left(\theta_{R_s}, \phi_{R_s}\right) \tag{25}$$

Taking derivative with respect to ξ, we have

$$I_2\left(n, m, i\xi, \bar{k}_i\right) = -\frac{1}{\sqrt{4\pi}} e^{-\xi R} \delta_{n0}\delta_{m0} - \left[j_n\left(i\xi R\right) + i\xi R j_n'\left(i\xi R\right)\right]$$

$$\sum_{s \neq 0} e^{i\bar{k}_i \cdot \bar{R}_s} (-1)^m h_n\left(i\xi R_s\right) Y_n^{(N)(-m)}\left(\theta_{R_s}, \phi_{R_s}\right)$$

$$-\xi j_n\left(i\xi R\right) \sum_{s \neq 0} i R_s e^{i\bar{k}_i \cdot \bar{R}_s} (-1)^m h_n'\left(i\xi R_s\right) Y_n^{(N)(-m)}\left(\theta_{R_s}, \phi_{R_s}\right) \tag{26}$$

Another derivative with ξ for $I_3(n, m, i\xi, \bar{k}_i)$ gives

$$\frac{d}{d\xi} I_2\left(n, m, i\xi, \bar{k}_i\right) = \frac{R}{\sqrt{4\pi}} e^{-\xi R} \delta_{n0}\delta_{m0}$$

$$- \left[2iR j_n'\left(i\xi R\right) - \xi R^2 j_n''\left(i\xi R\right)\right] \sum_{s \neq 0} e^{i\bar{k}_i \cdot \bar{R}_s} (-1)^m h_n\left(i\xi R_s\right) Y_n^{(N)(-m)}\left(\theta_{R_s}, \phi_{R_s}\right)$$

$$-2 \left[j_n\left(i\xi R\right) + i\xi R j_n'\left(i\xi R\right)\right] \sum_{s \neq 0} i R_s e^{i\bar{k}_i \cdot \bar{R}_s} (-1)^m h_n'\left(i\xi R_s\right) Y_n^{(N)(-m)}\left(\theta_{R_s}, \phi_{R_s}\right)$$

$$-\xi j_n\left(i\xi R\right) \sum_{s \neq 0} \left(-R_s^2\right) e^{i\bar{k}_i \cdot \bar{R}_s} (-1)^m h_n''\left(i\xi R_s\right) Y_n^{(N)(-m)}\left(\theta_{R_s}, \phi_{R_s}\right) \tag{27}$$

For $I_4(n, m, i\xi, \bar{k}_i)$, let $\bar{k}_{is}$ be represented by $\left|\bar{k}_{is}\right|$ and the angular directions $(\theta_{k_{is}}, \phi_{k_{is}})$

$$\bar{k}_{is} = \left|\bar{k}_{is}\right| \left(\sin\theta_{k_{is}} \cos\phi_{k_{is}} \hat{x} + \sin\theta_{k_{is}} \sin\phi_{k_{is}} \hat{y} + \cos\theta_{k_{is}} \hat{z}\right) \tag{28}$$

The plane wave expansion in spherical waves is [33]

$$e^{i\bar{k}_{is} \cdot \bar{r}} = 4\pi \sum_{n',m'} i^{n'} j_{n'}\left(\left|\bar{k}_{is}\right| R\right) Y_{n'}^{(N)m'}\left(\theta, \phi\right) Y_{n'}^{(N)(m')*}\left(\theta_{k_{is}}, \phi_{k_{is}}\right) \tag{29}$$

Substitute in the integral, we have

$$I_4\left(n, m, \bar{k}_{is}, \bar{k}_i\right) = 4\pi i^n j_n\left(\left|\bar{k}_{is}\right| R\right) Y_n^{(N)m*}\left(\theta_{k_{is}}, \phi_{k_{is}}\right) \tag{30}$$

Substitute in (18) we have

$$\tilde{D}_{nm}\left(k, \bar{k}_i\right) = -\frac{h_0^{(1)}\left(kR\right)}{j_0\left(kR\right)} \delta_{n0}\delta_{m0} + \frac{\sqrt{4\pi}}{ikj_n\left(kR\right)} I_1\left(n, m, i\xi, \bar{k}_i\right) - \frac{\sqrt{4\pi}}{ikj_n\left(kR\right)} \frac{\xi^2 + k^2}{2\xi} I_2\left(n, m, i\xi, \bar{k}_i\right)$$

$$+ \frac{\sqrt{4\pi}}{ikj_n\left(kR\right)} \frac{\left(\xi^2 + k^2\right)^2}{8\xi} I_3\left(n, m, i\xi, \bar{k}_i\right) + \frac{\sqrt{4\pi}}{ikj_n\left(kR\right)} \left(\xi^2 + k^2\right)^3 \sum_s \left[\frac{Q_{4n}^m\left(\bar{k}_{is}\right)}{\left(k_{is}^2 - k^2\right)}\right] \quad (31)$$

where

$$Q_{4n}^m\left(\bar{k}_{is}\right) = \frac{4\pi}{\Omega_0} i^n j_n\left(\left|\bar{k}_{is}\right| R\right) Y_n^{(N)(m)*}\left(\theta_{k_{is}}, \phi_{k_{is}}\right) \left[\frac{1}{\left(k_{is}^2 + \xi^2\right)^3}\right] \quad (32)$$

Note that we have used the index (n', m') to denote $\tilde{D}_{n'm'}(k, \bar{k}_i)$ to be consistent with the coefficients of exciting field and scattered field. The $\tilde{D}_{n'm'}(k, \bar{k}_i)$ can be computed rapidly for many wavenumbers k.

All the expansions are fast convergent. The expansion in $I_1(n, m, i\xi, \bar{k}_i)$, $I_2(n, m, i\xi, \bar{k}_i)$, $I_3(n, m, i\xi, \bar{k}_i)$ have exponential convergence since we have imaginary wavenumber $i\xi$. The last term has 8th order convergence in k_{is}^{-8}.

In the above expression of $\tilde{D}_{n'm'}(k, \bar{k}_i)$ in Equation (31), $I_1(n, m, i\xi, \bar{k}_i)$, $I_2(n, m, i\xi, \bar{k}_i)$, $I_3(n, m, i\xi, \bar{k}_i)$ and $Q_{4n'}^{m'}(\bar{k}_{is})$ are independent of k, making the expressions broadband as these quantities are computed once in the setup step. For wave expansions, the coefficients of the expansions are independent of R. For a given problem, the choice of R is such that all the required coefficients for the problem contribute to the wave expansion at that R. The choice of R in this paper is indicated in the section on numerical results. It has been shown in Tan and Tsang paper [19] that 8th order convergence gives Green's function accuracies to 3 to 4 significant figures which are sufficient for problems of interest. It was shown that for 3 to 4 significant figures of accuracies, the BBGF is much faster than Ewald's method for broadband calculations.

3. INTEGRAL EQUATIONS OF EXCITING FIELD AND SCATTERED FIELD IN MULTIPLE SCATTERING THEORY

The MST formulation is used to derive the integral equations. The derivations are done without the specifics of the scatterers. In Figure 2, consider a periodic lattice and let the lattice constant be a. Let the cells be labeled as (m, n, l). All the cells have the same scatterer placed in a background medium. Consider the $(0, 0, 0)$ cell. The scatterer is of arbitrary shape and is enclosed by a circular boundary S_B of radius b. Let S_C be the boundary of the $(0, 0, 0)$ cell. We use V_1 to denote region inside S_B and V_0 be the region outside the scatterer but within the cell $(0, 0, 0)$. Let ψ be the wave function in V_0. It satisfies the wave equation

$$\left(\nabla^2 + k^2\right) \psi\left(\bar{r}\right) = 0 \quad (33)$$

where $k = \omega/c$ is the wavenumber of the background medium, ω is the angular frequency and c is the wave velocity in the background medium. Setting c equal to unity, the normalized frequency is $f_N = k/(2\pi)$.

Based on multiple scattering theory (MST) [34–41], the wave function ψ is the sum of ψ^{ex}, the "final" exciting field, and ψ^s the "final" scattered field. Both ψ^{ex} and ψ^s refer to that of the "single scatterer" inside V_1. The self-consistent equations of MST allow ψ^{ex} and ψ^s to be calculated in a self-consistent manner.

$$\psi\left(\bar{r}\right) = \psi^{ex}\left(\bar{r}\right) + \psi^s\left(\bar{r}\right); \quad \text{for } \bar{r} \text{ in } V_0 \quad (34)$$

Because of extinction theorem $\psi^{ex}(\bar{r})$ is also defined in V_1. Thus, $\psi^{ex}(\bar{r})$ exists in V_0 and in V_1: The exciting field obeys the equation with the wavenumber k even though $\bar{r}$ can be in V_1.

$$\left(\nabla^2 + k^2\right) \psi^{ex}\left(\bar{r}\right) = 0 \quad \text{for } \bar{r} \text{ in } V_0 \text{ or in } V_1 \quad (35)$$
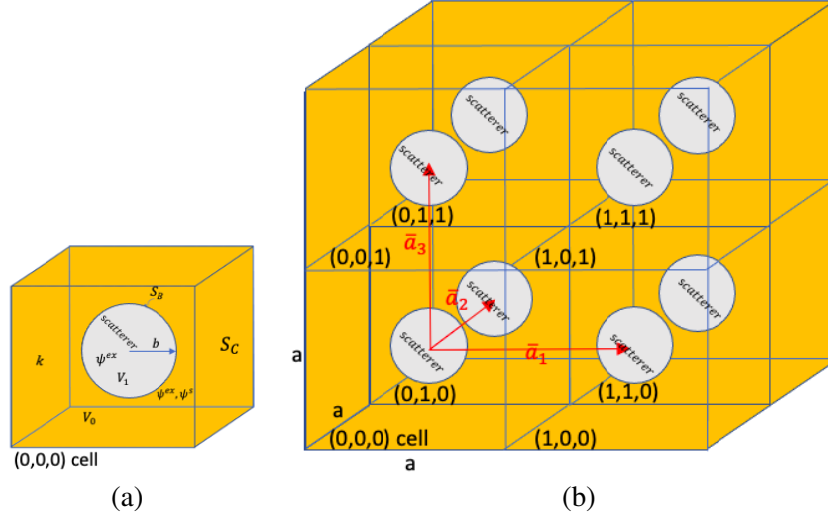
Figure 2. (a) The scatterer is of an arbitrary shape and is enclosed by a spherical boundary S_B of radius b about the origin. The origin is the center of the $(0, 0, 0)$ cell. Let S_C be the boundary of the $(0, 0, 0)$ cell. We use V_1 to denote region inside S_B and V_0 be the region outside the scatterer but within the cell $(0, 0, 0)$. (b) Periodic cubical cells with identical scatterers.

Because $\psi^s(\bar{r})$ is the scattered field from the single scatterer, it exists outside the scatterer. It exists in V_0 and outside the cell all the way to infinity.

$$\left(\nabla^2 + k^2\right) \psi^s\left(\bar{r}\right) = 0 \quad \text{for } \bar{r} \text{ in } V_0 \text{ and to infinity} \tag{36}$$

We have the lattice Green's function $g_P(k, \bar{k}_i, \bar{r}, \bar{r}')$ in Equations (9) and (16). In cell $(0, 0, 0)$, the lattice Green's function $g_P(k, \bar{k}_i, \bar{r}, \bar{r}')$ can be written as a sum of the free space Green's function $g_0(k, \bar{r}, \bar{r}')$ and the response Green's function $g_R(k, \bar{k}_i, \bar{r}, \bar{r}')$. The $g_P(k, \bar{k}_i, \bar{r}, \bar{r}')$ is the periodic Green's function for an empty lattice where the field point $\bar{r}$ and source point $\bar{r}'$ can be in V_0 or V_1.

$$g_P\left(k, \bar{k}_i, \bar{r}, \bar{r}'\right) = g_0\left(k, \bar{r}, \bar{r}'\right) + g_R\left(k, \bar{k}_i, \bar{r}, \bar{r}'\right) \tag{37}$$

We derived in [8] that for $\bar{r}$ in V_1 or in V_0.

$$\psi^{ex}\left(\bar{r}\right) = \int_{S_B} dS' \left[\psi^s\left(\bar{r}'\right) \hat{n}' \cdot \nabla' g_R\left(k, \bar{k}_i, \bar{r}, \bar{r}'\right) - g_R\left(k, \bar{k}_i, \bar{r}, \bar{r}'\right) \hat{n}' \cdot \nabla' \psi^s\left(\bar{r}'\right)\right] \tag{38}$$

The physical interpretation of Equation (38) is that the scattering from other cells into cell $(0, 0, 0)$ gives the exciting field on the scatterer in cell $(0, 0, 0)$. This agrees with what is stated in MST that the exciting field is the sum of incident field and scattered field from all other scatterers except itself [34–41]. For the band eigenvalue and band field problem, there is no incident field.

To solve the integral equation, we use spherical wave expansions of the exciting field and the scattered field. The final scattered field, in V_0 and all the way to infinity, can be expressed as outgoing spherical waves.

$$\psi^s\left(\bar{r}\right) = \sum_{n_1=0}^{N_L} \sum_{m_1} a_{n_1 m_1}^s \psi_{n_1 m_1}\left(k\bar{r}\right) \tag{39}$$

The summation of the expansion is to $|n| = N_L$. The key in MST is the convergence of the final scattered field. We note that the band eigen-frequencies are usually in the range of $0 \leq f_N \leq 1.5$. In photonic crystal, the size of the scatterer is of small or moderate size compared with wavelength. Thus, the maximum spherical wave index N_L is not large. The exciting field, as given in Equations (13) and (20) are in two regions V_1 and V_0. The expansions are in two regions. For $\bar{r}$ in V_1

$$\psi^{ex}\left(\bar{r}\right) = \sum_{n=0}^{N_L} \sum_m a_{nm} Rg\psi_{nm}\left(k\bar{r}\right) \tag{40}$$

The exciting field expansion, because of the Bessel function $j_n(kr)$, is a non-uniform convergent series. Since $\bar{r}$ is in V_1 in Equation (38), we need only to match to the scattered field with the maximum index to N_L.

For $\bar{r}$ in V_0, the r is much larger as it extends to the cell boundary. The argument of the Bessel function can be much larger. We need to have more terms with a larger upper index of N_{sph} in the expansion. Thus, we have

$$\psi^{ex}(\bar{r}) = \sum_{n=0}^{N_{sph}} \sum_m a_{nm}^C Rg\psi_{nm}(k\bar{r}) \quad \text{for } \bar{r} \text{ in } V_0 \tag{41}$$

where $N_{sph} \geq N_L$. We use two different symbols for the coefficients, a_{nm} and a_{nm}^C, to distinguish the two regions. Note that in Equation (39) we use index (n_1, m_1) for scattered field coefficients $a_{n_1 m_1}^s$ and the summation over n_1 up to N_L.

For the exciting field coefficients, we use index (n, m). The summation for exciting field over n is to N_L for V_1, meaning that the exciting field and scattered field have the same number of coefficients when applied to extinction theorem. For exciting field in V_0 the summation over n is to N_{sph}, where $N_{sph} \geq N_L$.

In view of Equation (16),

$$g_P\left(k, \bar{k}_i, \bar{r}, \bar{r}'\right) = \frac{ik}{\sqrt{4\pi}}\psi_{00}(k(\bar{r} - \bar{r}')) + \frac{ik}{\sqrt{4\pi}}\sum_{nm}\tilde{D}_{nm}\left(k, \bar{k}_i\right) Rg\psi_{nm}\left(k(\bar{r} - \bar{r}')\right) \tag{42}$$

The response Green's function is

$$g_R\left(k, \bar{k}_i, \bar{r}, \bar{r}'\right) = \frac{ik}{\sqrt{4\pi}}\sum_{nm}\tilde{D}_{nm}\left(k, \bar{k}_i\right) Rg\psi_{nm}\left(k(\bar{r} - \bar{r}')\right) \tag{43}$$

4. THE KKR EIGEN VALUE EQUATION

To perform the surface integral $\int_{S_B} dS'$ with $r' = b$ which is over the spherical surface of radius b, we make use of the addition theorem [38–40, 42–45].

$$Rg\psi_{nm}\left(k, (\bar{r} - \bar{r}')\right)\big|_{\bar{r} = \bar{r}'' - \bar{r}'} = \sqrt{4\pi}\sum_{n',m'}\sum_{n'',m''}(-1)^{m'}P\left(n'', m'', n', -m', n, m\right)Rg\psi_{n'm'}\left(k\bar{r}'\right)Rg\psi_{n''m''}\left(k\bar{r}\right) \tag{44}$$

where

$$P\left(n'', m'', n', -m', n, m\right)$$
$$= (-1)^{m'}(-1)^m(-1)^{n'}i^{n'+n''-n}\sqrt{(2n+1)(2n'+1)(2n''+1)}\begin{pmatrix} n & n' & n'' \\ 0 & 0 & 0 \end{pmatrix}\begin{pmatrix} n & n' & n'' \\ -m & m' & m'' \end{pmatrix} \tag{45}$$

In Equation (45), $\begin{pmatrix} n & n' & n'' \\ -m & m' & m'' \end{pmatrix}$ denotes the Wigner 3j symbols [39, 40, 42–45]. More details of $P(n, m, n_1, m_1, n', m')$ are given in Appendix B.

The response Green's function and normal derivative on the surface of S_B, with $|\bar{r}'| = b$ are respectively

$$g_R\left(k, \bar{k}_i, \bar{r}, \bar{r}'\right)\big|_{|\bar{r}'|=b} = ik\sum_{nm}\tilde{D}_{nm}\left(k, \bar{k}_i\right)\sum_{n',m'}\sum_{n'',m''}(-1)^{m'}P\left(n'', m'', n', -m', n, m\right)j_{n'}(kb)$$
$$Y_{n'}^{(N)m'}\left(\theta', \phi'\right)j_{n''}(kr)Y_{n''}^{(N)m''}\left(\theta, \phi\right) \tag{46}$$

$$\hat{n}' \cdot \nabla' g_R\left(k, \bar{k}_i, \bar{r}, \bar{r}'\right)\big|_{|\bar{r}'|=b} = ik^2\sum_{nm}\tilde{D}_{nm}\left(k, \bar{k}_i\right)\sum_{n',m'}\sum_{n'',m''}(-1)^{m'}P\left(n'', m'', n', -m', n, m\right)j_{n'}'(kb)$$
$$Y_{n'}^{(N)m'}\left(\theta', \phi'\right)j_{n''}(kr)Y_{n''}^{(N)m''}\left(\theta, \phi\right) \tag{47}$$

For the scattered field on the surface and the normal derivatives, we have

$$\psi^s\left(\bar{r}'\right)\big|_{|\bar{r}'|=b} = \sum_{n_1,m_1} a^s_{n_1 m_1} h^{(1)}_{n_1}\left(kb\right) Y^{(N)m_1}_{n_1}\left(\theta',\phi'\right) \tag{48}$$

$$\hat{n}'\cdot\nabla'\psi^s\left(\bar{r}'\right)\big|_{|\bar{r}'|=b} = \sum_{n_1,m_1} a^s_{n_1 m_1} h^{(1)'}_{n_1}\left(kb\right) Y^{(N)m_1}_{n_1}\left(\theta',\phi'\right) \tag{49}$$

Note that for ψ^s, we use index (n_1, m_1) for coefficients.

Substitute in and carry out the integration $\int_{S_B} dS' = b^2 \int_0^\pi d\theta' \sin\theta' \int_0^{2\pi} d\phi'$. We also use orthonormality of spherical harmonics.

$$\int_S dS'\, \psi^s\left(\bar{r}'\right)\left[\hat{n}'\cdot\nabla' g_R\left(k,\bar{k}_i,\bar{r},\bar{r}'\right)\right]\big|_{|\bar{r}'|=b}$$
$$= ik^2 b^2 \sum_{n_1,m_1} a^s_{n_1 m_1} h^{(1)}_{n_1}\left(kb\right) \sum_{nm} \tilde{D}_{nm}\left(k,\bar{k}_i\right) \sum_{n'',m''}$$
$$P\left(n'',m'',n_1,m_1,n,m\right) j'_{n_1}\left(kb\right) j_{n''}\left(kr\right) Y^{(N)m''}_{n''}\left(\theta,\phi\right) \tag{50}$$

Similarly

$$-\int_{S_B} dS'\, g_R\left(k,\bar{k}_i,\bar{r},\bar{r}'\right)\left[\hat{n}'\cdot\nabla'\psi^s\left(\bar{r}'\right)\right]\big|_{|\bar{r}'|=b}$$
$$= -ik^2 b^2 \sum_{n_1,m_1} a^s_{n_1 m_1} h^{(1)'}_{n_1}\left(kb\right) \sum_{nm} \tilde{D}_{nm}\left(k,\bar{k}_i\right) \sum_{n'',m''}$$
$$P\left(n'',m'',n_1,m_1,n,m\right) j_{n_1}\left(kb\right) j_{n''}\left(kr\right) Y^{(N)m''}_{n''}\left(\theta,\phi\right) \tag{51}$$

Adding the two terms and making use of the Wronskian [46], $h^{(1)}_n\left(\omega\right) j'_n\left(\omega\right) - h^{(1)'}_n\left(\omega\right) j_n\left(\omega\right) = -\frac{i}{\omega^2}$.

$$\int_S dS'\, \psi^s\left(\bar{r}'\right)\left[\hat{n}'\cdot\nabla' g_R\left(k,\bar{k}_i,\bar{r},\bar{r}'\right)\right]\big|_{|\bar{r}'|=b} - \int_{S_B} dS'\, g_R\left(k,\bar{k}_i,\bar{r},\bar{r}'\right)\left[\hat{n}'\cdot\nabla'\psi^s\left(\bar{r}'\right)\right]\big|_{|\bar{r}'|=b}$$
$$= \sum_{n_1,m_1} a^s_{n_1 m_1} \sum_{nm} \tilde{D}_{nm}\left(k,\bar{k}_i\right) \sum_{n'',m''} P\left(n'',m'',n_1,m_1,n,m\right) j_{n''}\left(kr\right) Y^{(N)m''}_{n''}\left(\theta,\phi\right) \tag{52}$$

From Equation (38), for $\bar{r}$ in V_1 or in V_0 Equation (52) is the exciting field of the scatterer in cell $(0, 0, 0)$. The exciting field is the scattered field from scatterers of all other cells except $(0, 0, 0)$ into cell $(0, 0, 0)$. Thus, the number of terms differ whether $\bar{r}$ is in region V_0 or in V_1.

$$\psi^{ex}\left(\bar{r}\right) = \int_{S_B} dS'\left[\psi^s\left(\bar{r}'\right)\hat{n}'\cdot\nabla' g_R\left(k,\bar{k}_i,\bar{r},\bar{r}'\right) - g_R\left(k,\bar{k}_i,\bar{r},\bar{r}'\right)\hat{n}'\cdot\nabla'\psi^s\left(\bar{r}'\right)\right]$$
$$= \sum_{n'',m''}\left[\sum_{n_1,m_1} a^s_{n_1 m_1} \sum_{nm} \tilde{D}_{nm}\left(k,\bar{k}_i\right) P\left(n'',m'',n_1,m_1,n,m\right)\right] j_{n''}\left(kr\right) Y^{(N)m''}_{n''}\left(\theta,\phi\right)$$
$$= \begin{cases} \sum_{n''=0}^{N_L}\sum_{m''} a_{n''m''} j_{n''}\left(kr\right) Y^{(N)m''}_{n''}\left(\theta,\phi\right) & \text{for } \bar{r} \text{ in } V_1 \\[2em] \sum_{n''=0}^{N_{sph}}\sum_{m''} a^C_{nm} j_{n''}\left(kr\right) Y^{(N)m''}_{n''}\left(\theta,\phi\right) & \text{for } \bar{r} \text{ in } V_0 \end{cases} \tag{53}$$

For the eigenvalue equation, which is the KKR equation, we apply extinction theorem for $\bar{r}$ in V_1. For $\bar{r}$ in V_1, we write $\psi^{ex}(\bar{r}) = \sum_{n'',m''} a_{n''m''} j_{n''}(kr) Y^{(N)m''}_{n''}(\theta,\phi)$. We then balance the coefficients of spherical waves of $j_{n''}(kr) Y^{(N)m''}_{n''}(\theta,\phi)$.

$$a_{n''m''} = \sum_{n_1,m_1} a^s_{n_1 m_1} \sum_{nm} P\left(n'',m'',n_1,m_1,n,m\right) \tilde{D}_{nm}\left(k,\bar{k}_i\right) \tag{54}$$

Let

$$d_{nmn_1m_1}\left(k,\bar{k}_i\right) = \sum_{n'm'} P\left(n,m,n_1,m_1,n',m'\right)\tilde{D}_{n'm'}\left(k,\bar{k}_i\right) \tag{55}$$

Changing dummy variables gives

$$a_{nm} = \sum_{n_1=0}^{N_L}\sum_{m_1=-n_1}^{n_1} d_{nmn_1m_1}\left(k,\bar{k}_i\right)a_{n_1m_1}^s; \quad n = 0,1,...,N_L; \ m = 0,\pm1,...,\pm n \tag{56}$$

Equation (56) is labelled as the KKR eigenvalue equation. Note that although the right-hand sides of Equations (55) and (56) require summation of $\sum_{n_1,m_1}\sum_{n'm'}$, there are relatively few terms in the summation. This is because in photonic crystal the size of the scatterer is not large. Equation (54) is a result of extinction theorem inside V_1 of the scatterer. We only need to limit to $n = N_L$ with $m = 0,\pm1,...,\pm n$. In photonic crystals, N_L is usually at most 4.

In the KKR eigenvalue equation the index n for the exciting field is up to N_L. The index for the scattered field, the summation over n_1 is to N_L. Because of the properties of Wigner 3j symbols (Appendix C), $|n - n_1| \leq n' \leq n + n_1$. Thus, n' is up to $N_L + N_L = 2N_L$.

For the extinction theorem,

$$d_{nmn_1m_1}\left(k,\bar{k}_i\right) = \sum_{n'=0}^{2N_L}\sum_{m'=-n'}^{n'} P\left(n,m,n_1,m_1,n',m'\right)\tilde{D}_{n'm'}\left(k,\bar{k}_i\right) \tag{57}$$

5. SINGLE SCATTERER T MATRIX AND KKR EIGENVALUE EQUATION

In MST, the relation between the "final" scattered field coefficient and the "final" exciting field coefficient is the single scatterer T matrix. The T matrix is a convenient representation because it is the scattering T matrix that is for an isolated single scatterer [38–41, 47]. The T matrix is independent of the lattice and is independent of the Bloch vector $\bar{k}_i$. The T matrix is dependent on wavenumber k.

Then

$$a_{n_1m_1}^s = \sum_{n=0}^{N_L}\sum_{m=-n}^{n} T_{n_1m_1nm}\left(k\right)a_{nm}; \quad n_1 = 0,1,...,N_L; \ m_1 = 0,\pm1,...,\pm n_1 \tag{58}$$

In this equation, both exciting field and scattered field are with n and n_1 to N_L. The dimension of the T matrix is not large because scatterers in photonic crystals are not large compared to wavelength.

We use a combined index l to represent (n,m) with $l = n^2 + (n + m + 1)$. The index $l = 1,2,...,L$ where $L = (1 + 3 + 5 + ..., +(2N_L + 1)) = (N_L + 1)^2$. The Equations (56) and (58) become, respectively,

$$a_l = \sum_{l_1=1}^{L} d_{ll_1}\left(k,\bar{k}_i\right)a_{l_1}^s; \quad l = 0,1,...,L \tag{59}$$

$$a_{l_1}^s = \sum_{l=1}^{L} T_{l_1l}\left(k\right)a_l; \quad l = 0,1,...,L \tag{60}$$

We next cast (59) and (60) in matrix notations. Using matrix notations of $a_l \to \bar{a}$, $a_l^s \to \bar{a}^s$, $T_{ll'}(k) \to \bar{\bar{T}}(k)$, and $\bar{\bar{d}}(k,\bar{k}_i)$ with dimension $L \times 1$ for column vectors and dimension $L \times L$ for matrices

$$\bar{a} = \bar{\bar{d}}\left(k,\bar{k}_i\right)\bar{a}^s \tag{61}$$

$$\bar{a}^s = \bar{\bar{T}}\left(k\right)\bar{a} \tag{62}$$

The eigenvalue equation is

$$\bar{\bar{S}}\left(k,\bar{k}_i\right)\bar{a} = 0 \tag{63}$$

where

$$\bar{\bar{S}}\left(k,\bar{k}_i\right) = \bar{\bar{I}} - \bar{\bar{d}}\left(k,\bar{k}_i\right)\bar{\bar{T}}\left(k\right) \tag{64}$$

and $\overline{\overline{I}}$ is the $L \times L$ unit matrix.

The eigenvector in Equation (63) is the exciting field coefficients $\bar{a}$. Next, we convert the eigenvalue equation into one with eigenvector $\bar{a}^s$. Let $\overline{\overline{t}}$ be related to the inverse of the T matrix.

$$\overline{\overline{t}}(k) = i\left(\overline{\overline{I}} + \overline{\overline{T}}^{-1}(k)\right) \tag{65}$$

Then

$$\overline{\overline{\Lambda}}\left(k, \bar{k}_i\right) \bar{a}^s = 0 \tag{66}$$

where

$$\overline{\overline{\Lambda}}\left(k, \bar{k}_i\right) = \overline{\overline{D}}\left(k, \bar{k}_i\right) - \frac{1}{4}\overline{\overline{t}}(k) \tag{67}$$

$$\overline{\overline{D}}\left(k, \bar{k}_i\right) = \frac{i}{4}\left(\overline{\overline{d}}\left(k, \bar{k}_i\right) + \overline{\overline{I}}\right) \tag{68}$$

The eigenvalue is calculated from KKR eigenvalue equation of (66) by an iterative search in k. Let k_e be the eigenvalue. Then $\bar{a}^s(k_e)$, the eigenvector is found after the eigenvalue is obtained. The eigenvector is normalized with respect to the KKR eigenvalue equation of (66). However, on the other hand, the band field solution is normalized by volumetric integration of the band field wave function. In MST, it is advantageous to use scattered field coefficients $\bar{a}^s$. The expansion of the scattered field is uniform convergence. The expansion of the exciting field is non-uniformly convergent. The use of exciting field expansion is to obtain the scattered field coefficients by matching boundary conditions. These considerations are clear in the tables of coefficients in the numerical results section. Thus, in solving eigenvalue problem, we use Equation (66) and not Equation (63).

6. HIGHER ORDER SPHERICAL WAVES OF BAND FIELD SOLUTIONS

The eigenvalue equation is obtained by imposing boundary conditions on the surface of the scatterer. The size of the matrix with maximum $n = N_L$ is based on the size of the T matrix. Thus, only a small value of N_L is required. After the eigenvalue k_e is obtained, the normalized eigenvector as $\bar{a}^s(k_e)$, which is $\bar{a}^s_{n_1,m_1}(k_e)$, is calculated which has maximum n equal to N_L. We use index (n_1, m_1) to denote scattered field coefficient.

To calculate the band field wave function over the entire unit cell, higher order spherical waves are required as maximum r in the $(0,0,0)$ is $r_{\max} = \sqrt{3}a/2$ which can be much larger than the the radius b of V_1.

We shall use maximum $n = N_{sph}$ for band field wave function in the $(0,0,0)$ cell. The exciting field is due to scattering from other cells into the cell $(0,0,0)$. We have, from Equation (53),

$$\psi_{ex}^C\left(k_e, \bar{r}\right) = \sum_{n=0}^{N_{sph}} \sum_m$$

$$\left[\sum_{n_1=0}^{N_L} \sum_{m_1} a^s_{n_1 m_1}(k_e) \sum_{n'}^{N_{sph}+N_L} \sum_{m'} \tilde{D}_{n'm'}\left(k_e, \bar{k}_i\right) P\left(n, m, n_1, m_1, n', m'\right)\right] j_n\left(k_e r\right) Y_n^{(N)m}\left(\theta, \phi\right) \tag{69}$$

where superscript "C" represents higher order spherical waves. The summation of scattered field $a^s_{n_1 m_1}(k_e)$ is up to N_L which is available from the eigenvector. Since n is up to N_{sph}, we need to calculate higher order $P(n, m, n_1, m_1, n', m')$ and $\tilde{D}_{n'm'}(k_e, \bar{k}_i)$. The calculation of higher order $\tilde{D}_{n'm'}(k_e, \bar{k}_i)$ is at the single eigenvalue wavenumber k_e. Because of the property of the Wigner 3j coefficients (Appendix B), n' is up to the sum of maximum n and maximum n_1. Thus, n' is up to $N_{sph} + N_L$. Then

$$\psi_{ex}^C\left(k_e, \bar{r}\right) = \sum_{n=0}^{N_{sph}} \sum_m a_{nm}^C\left(k_e\right) j_n\left(k_e r\right) Y_n^{(N)m}\left(\theta, \phi\right) \tag{70}$$

where

$$a_{nm}^C (k_e) = \sum_{n_1=0}^{N_L} \sum_{m_1} d_{nmn_1m_1}^C (k_e) a_{n_1m_1}^s (k_e) \tag{71}$$

$$d_{nmn_1m_1}^C (k_e) = \sum_{n'}^{N_{sph}+N_L} \sum_{m'} \tilde{D}_{n'm'} (k_e) P(n, m, n_1, m_1, n', m'); \quad n = 0, ..., N_{sph}; \ n_1 = 0, ..., N_L \tag{72}$$

In matrix notation

$$\bar{a}^C (k_e) = \bar{\bar{d}}^C (k_e) \bar{a}^s (k_e) \tag{73}$$

where $\bar{\bar{d}}^C (k_e)$ is now a rectangular matrix. We can further obtain the "C" higher order version of the scattered field coefficients at the eigenvalue k_e by

$$\bar{a}^{sC} (k_e) = \bar{\bar{T}}^C (k_e) \bar{a}^C (k_e) \tag{74}$$

where $\bar{\bar{T}}^C (k_e)$ is the square matrix with T matrix coefficients at k_e and calculated up to maximum $n = N_{sph} + N_L$.

The higher order scattered wave is

$$\psi_s^C (k_e, \bar{r}) = \sum_{n=0}^{N_{sph}} \sum_m a_{nm}^{sC} (k_e) h_n^{(1)} (k_e r) Y_n^{(N)m} (\theta, \phi) \tag{75}$$

As we show in the numerical result section, the higher order scattered field $a_{nm}^{sC}(k_e)$ are small as expected. The field in region V_0 is

$$\begin{aligned} \psi^C (k_e, \bar{r}) &= \psi_{ex}^C (k_e, \bar{r}) + \psi_s^C (k_e, \bar{r}) \\ &= \sum_{n=0}^{N_{sph}} \sum_m \left[a_{nm}^C (k_e) j_n (k_e r) + a_{nm}^{sC} (k_e) h_n^{(1)} (k_e r) \right] Y_n^{(N)m} (\theta, \phi) \end{aligned} \tag{76}$$

For the case of spherical scatterer of radius b, let the wavenumber $k_{pe} = \sqrt{\frac{\varepsilon_p}{\varepsilon}} k_e$ where ε_p is the permittivity of the scatterer and ε the permittivity of the background. For the case of scalar wave, we ignore the polarization effects. In such a case, $\sqrt{\frac{\varepsilon_p}{\varepsilon}}$ is the relative refractive index of the scatterer relative to the background. The field inside the particle is

$$\psi_p^C (k_e, \bar{r}) = \sum_{n,m} c_{nm}^C (k_e) j_n (k_{pe} r) Y_n^{(N)m} (\theta, \phi) \tag{77}$$

with

$$c_{nm}^C (k_e) = \frac{a_{nm}^{sC} (k_e) h_n^{(1)} (k_e b) + a_{nm}^C (k_e) j_n (k_e b)}{j_n (k_{pe} b)} \tag{78}$$

7. NORMALIZATION OF BAND FIELDS

Consider two eigen-solutions β_1 and β_2 at $\bar{k}_i$. The two band field solutions are orthonormal.

$$\frac{\varepsilon}{\varepsilon_0} \int_{V_0} d\bar{r} \psi_{\beta_1} \psi_{\beta_2}^* + \frac{\varepsilon_p}{\varepsilon_0} \int_{V_1} d\bar{r} \psi_{p,\beta_1} \psi_{p,\beta_2}^* = \delta_{\beta_1\beta_2} \tag{79}$$

The normalization is

$$\frac{\varepsilon}{\varepsilon_0} \int_{V_0} d\bar{r} \left| \psi^C (k_e, \bar{r}) \right|^2 + \frac{\varepsilon_p}{\varepsilon_0} \int_{V_1} d\bar{r} \left| \psi_p^C (k_e, \bar{r}) \right|^2 = 1 \tag{80}$$

In Figure 3, the V_0 region is further divided into two regions so that $V_0 = V_{0c} + V_{0r}$. The V_{0c} consists of the spherical shell with $b \le r < \frac{a}{2}$ while V_{0r} is the remainder of the cell $(0, 0, 0)$.
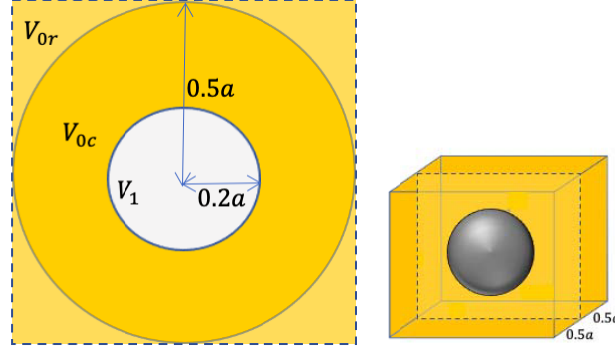
Figure 3. The middle-cut plot of the cube. V_1: $r < b$; $V_0 = V_{0c} + V_{0r}$. The V_{0c} consists of the spherical shell with $b \leq r < \frac{a}{2}$; V_{0r} is the remainder of V_0.

By making use of orthonormality of spherical harmonics (Appendix A) and the integral of product of spherical Bessel and Hankel functions [48], the integral over V_{0c} can be carried out analytically. For the integral over V_1, we consider the example of spherical scatterer and the integration can also be carried out analytically. It follows that

$$\frac{\varepsilon_p}{\varepsilon_0} \int_{V_1} d\bar{r} \left| \psi_p^C (k_e) \right|^2 = \frac{\varepsilon_p}{\varepsilon_0} \sum_{n,m} \left| c_{nm}^C (k_e) \right|^2 I_1(j_n, k_{pe}, 0, b) \tag{81}$$

$$\frac{\varepsilon}{\varepsilon_0} \int_{V_{0c}} d\bar{r} \left| \psi^C (k_e) \right|^2 = \frac{\varepsilon}{\varepsilon_0} \sum_{n,m} \left(\left| a_{nm}^C \right|^2 I_1 \left(j_n, k, b, \frac{a}{2} \right) + \left| a_{nm}^{sC} \right|^2 I_2 \left(h_n^{(1)}, h_n^{(2)}, k, b, \frac{a}{2} \right) \right.$$

$$\left. + 2\text{Re} \left(a_{nm}^{sC} a_{nm}^{C*} I_2 \left(j_n, h_n^{(1)}, k, b, \frac{a}{2} \right) \right) \right) \tag{82}$$

where

$$I_1 (z_n, \alpha, c, d) = \int_c^d dr r^2 (z_n (\alpha r))^2 = \left[\frac{r^3}{2} (z_n (\alpha r) z_n (\alpha r) - z_{n-1} (\alpha r) z_{n+1} (\alpha r)) \right]_{r=c}^{r=d} \tag{83}$$

$$I_2 (z_n, q_n, \alpha, c, d) = \int_c^d dr r^2 z_n (\alpha r) q_n (\alpha r) = \left[\frac{r^2}{2\alpha} \left(\alpha r z_n (\alpha r) q_n (\alpha r) - \alpha r z_{n-1} (\alpha r) q_{n+1} (\alpha r) \right. \right.$$

$$\left. \left. + \left(n + \frac{1}{2} \right) (-z_n (\alpha r) q_{n-1} (\alpha r) + z_{n-1} (\alpha r) q_n (\alpha r)) \right) \right]_{r=c}^{r=d} \tag{84}$$

In Equations (83) and (84), $z_n(\alpha r)$ and $q_n(\alpha r)$ can be any spherical Bessel function that includes j_n, n_n, $h_n^{(1)}$, and $h_n^{(2)}$.

8. NUMERICAL RESULTS AND DISCUSSIONS

We choose simple cubic lattice (Figure 1) with the lattice constant $a = 1$. The radius of the spherical scatterer is $b = 0.2a$. The background permittivity is $\varepsilon = \varepsilon_0$. The scatterer has permittivity $\varepsilon_p = 8.9\varepsilon_0$.

The speed of light is chosen as $c = 1$. We shall first illustrate the calculations of the band eigenvalue and band field at the point X in the first Brillouin zone.

For the point X, $\bar{k}_i = 0.5\bar{b}_1$ which means $(\beta_1, \beta_2, \beta_3) = (0.5, 0, 0)$. We will also illustrate the band diagram for the first 2 bands with $0 \leq \beta_1 \leq 0.5, \beta_2 = \beta_3 = 0$.

In the calculations of the broadband spherical wave coefficients $\tilde{D}_{n'm'}(k, \bar{k}_i)$ with imaginary extractions, we use $N_{spa} = 2$, $N_{spe} = 3$, $\xi = \frac{2\pi}{a}$, $R = 0.5a$.

8.1. Eigenvalue and Normalized Eigenvector at Point X

The eigenvalue part is the CPU intensive part of the method. Based on discussion in the previous section, we choose a low $N_L = 1$. Then maximum $n = 1$ for the exciting field coefficient. The maximum $n_1 = 1$ is also for the scattered field coefficient. The maximum $n' = 2$ for $\tilde{D}_{n'm'}(k, \bar{k}_i)$. We have 4 pairs of $(n, m) = (0, 0), (1, -1), (1, 0)$, and $(1, 1)$. Thus, the dimension of the eigenvalue equation is 4. We use a combined index l to represent (n, m) with dimension of the matrix of the KKR eigenvalue equation, $\overline{\overline{\Lambda}}(k)\bar{a}^s = 0$, with $l_{\max} = 4$. It shows that the eigenvalue problem is stable with fewer terms in the expansions and fewer number of coefficients. It is because the eigenvalue problem was derived based on matching the boundary conditions on the surface of the scatterer. Thus, we use different numbers of terms in band eigenvalue problem and in band field solutions. The normalized frequency is $f_N(k) = \frac{k}{2\pi}\sqrt{\frac{\varepsilon_0}{\varepsilon}}$.

The frequency scanning approach is compared with the bisection method in searching for k. Table 1 is shown for the CPU time for the two methods. The determinant of $\overline{\overline{\Lambda}}(k)$ is a real number. We plot the sign of the determinant and the absolute value of the determinant as a function of f_N in Figures 4(a) and 4(b) respectively. The figure clearly shows that the two eigenvalues for the first 2 bands are $f_{Ne} = 0.3748$ and $f_{Ne} = 0.4868$, where "e" stands for eigenvalue. As shown in Table 1, the bisection method is fast as it requires only 0.27 seconds for the first two bands. It is interesting that the frequency scanning method requires only 2.92 seconds for 10000 frequencies. This indicates that many more bands than 2 bands can be calculated with 10000 frequencies in frequency scanning.

We will illustrate band field solutions for $f_{Ne} = 0.4868$. The wavenumber eigenvalue is $k_e = 3.058$.
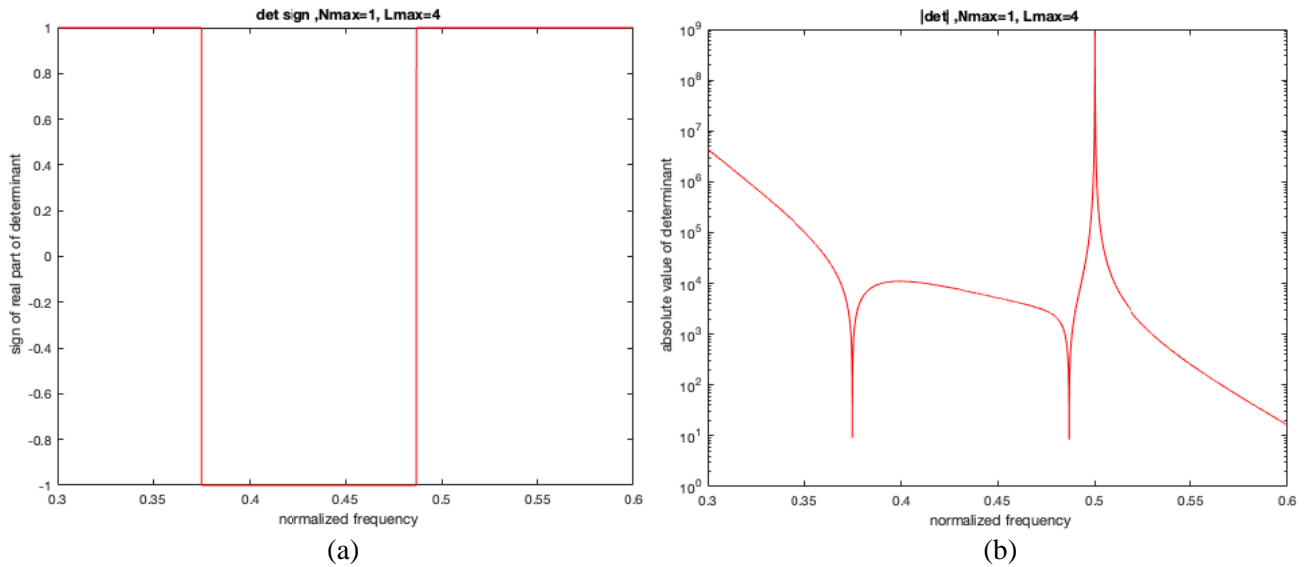

(a) (b)

Figure 4. Normalized frequency response of (a) sign of determinant, (b) absolute value of determinant.

Table 1. CPU simulation time breakdown table for frequency scanning method and bisection method (1.8 GHz Dual-Core Intel Core i5; 8 GB 1600 MHz DDR3).

Method	Number of bands	$(N_{\mathbf{max}}, N_{\mathbf{1,max}}, N_{\mathbf{p,max}})$	Set-up (milli-sec)	Number of frequencies	$\tilde{D}$ and $\det(\mathbf{\Lambda})$ (milli-sec)	Total CPU (sec)
Frequency scanning	2	(1, 1, 2)	151.49	10000	2772.21	2.92
Bisection	2	(1, 1, 2)	154.91	28	114.44	~ 0.27

Table 2. Scattered field coefficients for $f_{Ne} = 0.4868$.

n	m	l	a^s_{nm}
0	0	1	0
1	−1	2	0.7071
1	0	3	0
1	1	4	−0.7071

The eigenvector for the 4 by 4 eigenvalue problem is for the scattered field coefficients, a^s_{nm}, as shown in Table 2.

The eigenvector a^s_{nm} is normalized so that $\sum_{nm} \sqrt{(a^s_{nm})^2} = 1$. Note that this is normalization of the eigenvector for the matrix equation and is not the normalization of the band field solution which will be calculated later.

8.2. Higher Order Spherical Waves

After the eigenvalue and eigenvector of the scattered field coefficients are obtained, we calculate the band field solutions for the entire $(0,0,0)$ cell. This requires higher order coefficients. We calculate up to $n = N_{sph} = 5$ with $L_{max} = 36$. The majority of the coefficients are small. The significant ones are illustrated in Table 3.

The higher order scattering coefficients a^{sC}_{nm} are small. The higher order exciting coefficients a^C_{nm} and internal field coefficients c^C_{nm} have larger values. However, the contributions to the band field solutions are the products of the coefficients and Bessel function, viz. $a^C_{nm} j_n(k_e r)$ and $c^C_{nm} j_n(k_{pe} r)$ and not the coefficients alone. In the $(0,0,0)$ cell $r_{max} = 0.866a$, so that $(k_e r)_{max} = 2.64$. This means that the contributions of spherical waves to the band field solutions with $n = 5$ are small.

8.3. Normalization of Wave Functions

Then we calculate the normalization integrals. The normalization for the wave functions is the square root of the sum of the 3 integrals in Table 4 which is $\sqrt{34.358} = 5.861$. The factor is used to normalize the coefficients. The normalized coefficients are in parenthesis in the above Table 3.

8.4. The Band Field Solution

We next plot the band field solution using the normalized coefficients of exciting field, scattered field, and internal field from Equations (76) and (77).

In Figure 5, we plot the band field solution along the center line for $(x, 0, 0)$ where $-\frac{a}{2} \leq x \leq \frac{a}{2}$. The red and blue are real and imaginary parts of the higher order solution. The low order solution includes only $(n, m) = (1, -1)$ and $(n, m) = (1, 1)$. The low order solution has the simple form.

$$\psi^C (k_e, \bar{r}) = \frac{\sqrt{3}}{\sqrt{2\pi}} i \left[5.776 j_1 (3.058r) - 0.12 n_1 (3.058r) \right] \sin\theta \cos\phi \tag{85}$$

$$\psi^C_p (k_e, \bar{r}) = \frac{\sqrt{3}}{\sqrt{2\pi}} i (3.529) j_1 (9.124r) \sin\theta \cos\phi \tag{86}$$

Figure 5 shows that the low order solution is accurate up to the vicinity of the scatterer. At the boundary of the scatterer $r = b = 0.2a$, the difference between high order and low order is 2%. This shows that $N_L = 1$ is of sufficient accuracy for the eigenvalue problem because the eigenvalue problem requires only that the boundary conditions on the surface the scatterer is obeyed. However, if the entire curves within $-0.5a$ to $0.5a$ are considered, L^2-norm between high order and low order is up to 10%. This shows that for field further than the scatterer, we need to use higher order spherical waves to calculate the scattered fields in the entire $(0, 0, 0)$. Figure 6 shows slices of 3-D field solutions.
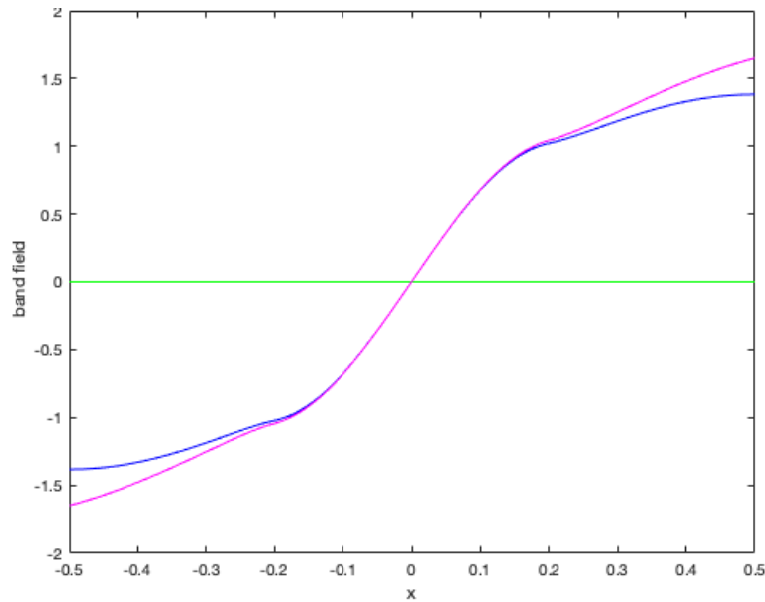
Figure 5. Band field solution along the center line for low order solution includes only $(n, m) = (1, -1)$ and $(n, m) = (1, 1)$; Red and blue lines are for higher order. Green and Magenta lines are for low order. Green line overlaps red line.
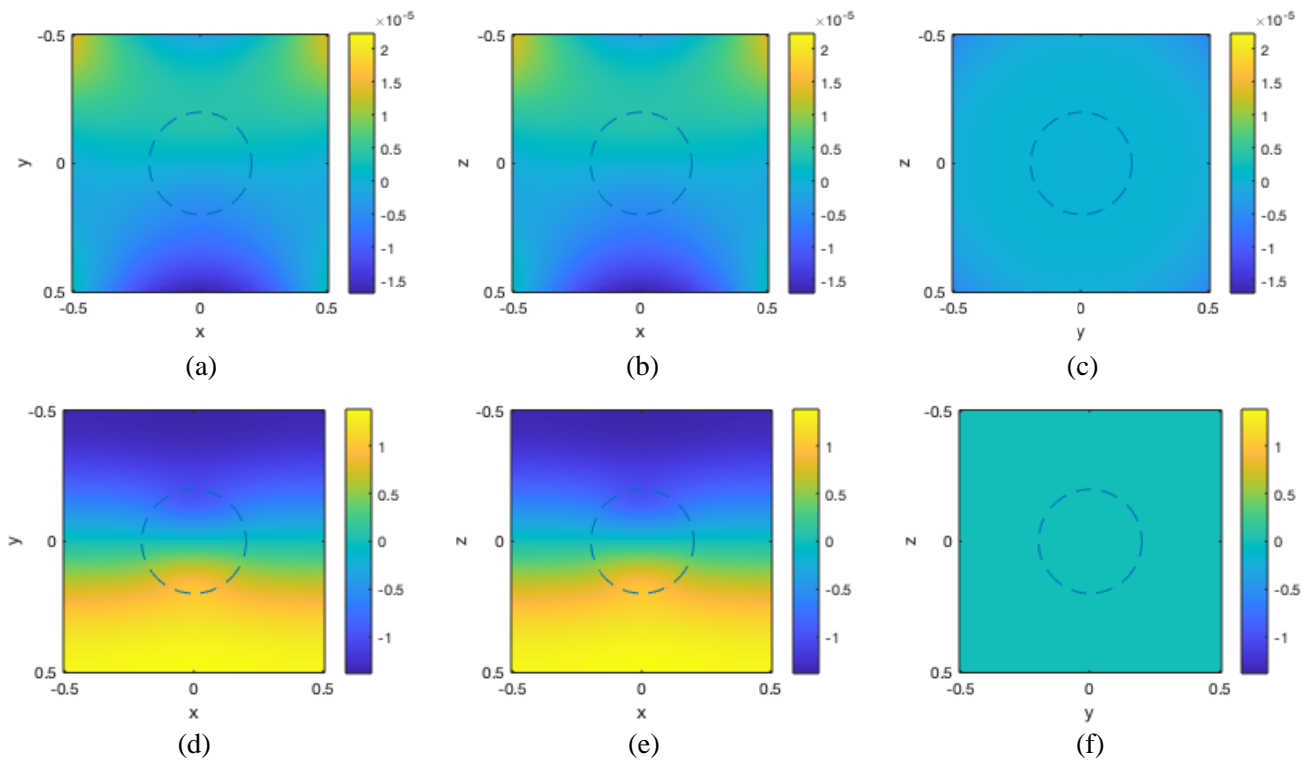

Figure 6. 2-D slices of 3-D field solution for $f_{Ne} = 0.4868$ at X-point in $(0, 0, 0)$ cell, (a) real part of 2-D slice for $z = 0$, (b) real part of 2-D slice for $y = 0$, (c) real part of 2-D slice for $x = 0$, (d) imaginary part of 2-D slice for $z = 0$, (e) imaginary part of 2-D slice for $y = 0$, (f) imaginary part of 2-D slice for $x = 0$.

Table 3. Scattering coefficients inside and outside the scatterer: There are 2 numbers, first is normalized eigen vector for matrix equation; number in parenthesis is normalized band field solution.

n	m	l	a_{nm}^c	(a_{nm}^{sC})	c_{nm}^C
1	-1	2	$-0.7071 - 33.83i$	0.7073	$-20.6742i$
			$(-0.1206 - 5.7721i)$	(0.1207)	$(-3.5274i)$
1	1	4	$0.7071 + 33.8391i$	-0.7073	$20.6742i$
			$(0.1206 + 5.7736i)$	(-0.1207)	$(3.5274i)$
3	-3	10	$42.4043i$	$-42.4661e - 06$	$1.9867i$
			$(7.2350i)$	$(-7.2455e - 06)$	$(0.3390i)$
3	-1	12	$-32.8463i$	$32.8941e - 06$	$-1.5389i$
			$(-5.6042i)$	$(5.6124e - 06)$	$(-0.2626i)$
3	1	14	$32.8463i$	$-32.8941e - 06$	$1.5389i$
			$(5.6042i)$	$(-5.6124e - 06)$	$(0.2626i)$
3	3	16	$-42.4043i$	$42.4661e - 06$	$-1.9867i$
			$(-7.2350i)$	$(7.2455e - 06)$	$(-0.3390i)$
5	-5	26	$-86.7455i$	$8.2850e - 10$	$-0.4207i$
			$(-14.8005i)$	$(1.4136e - 10)$	$(-0.0718i)$
5	-3	28	$41.1362i$	$-39.2889e - 11$	$0.1995i$
			$(7.0186i)$	$(-6.7034e - 11)$	$(0.0340i)$
5	-1	30	$-70.7478i$	$6.7571e - 10$	$-0.3431i$
			$(-12.0709i)$	$(1.1529e - 10)$	$(-0.0585i)$
5	1	32	$70.7478i$	$-6.7571e - 10$	$0.3431i$
			$(12.0709i)$	$(-1.1529e - 10)$	$(0.0585i)$
5	3	34	$-41.1362i$	$39.2889e - 11$	$-0.1995i$
			$(-7.0186i)$	$(6.7034e - 11)$	$(-0.0340i)$
5	5	36	$86.7455i$	$-8.2850e - 10$	$0.4207i$
			$(14.8005i)$	$(-1.4136e - 10)$	$(0.0718i)$

Table 4. Breakdown of integral of field solution for the normalization.

Integral	Normalization Integral
$\frac{\varepsilon_p}{\varepsilon_0} \int_{V_1} d\bar{r} \left| \psi_p^C (k_e, \bar{r}) \right|^2$	2.779
$\frac{\varepsilon}{\varepsilon_0} \int_{V_{0c}} d\bar{r} \left| \psi^C (k_e, \bar{r}) \right|^2$	11.968
$\frac{\varepsilon}{\varepsilon_0} \int_{V_{0r}} d\bar{r} \left| \psi^C (k_e, \bar{r}) \right|^2$	19.612
sum	34.358

8.5. Band Diagram

In Figure 7, we plot the band diagram for the first two bands between Γ and X points in the first Brillouin zone for $\beta_2 = \beta_3 = 0$ and $0 \leq \beta_1 \leq \frac{\pi}{2}$. The lower band is close to a straight line near Γ point meaning that an effective permittivity can be derived. The band eigenvalue frequencies are given in the following Table 5 for X point and Γ point. Usually the first band near the Γ point can be derived using low frequency method or quasistatic solution. The second band is beyond the quasistatic solution.
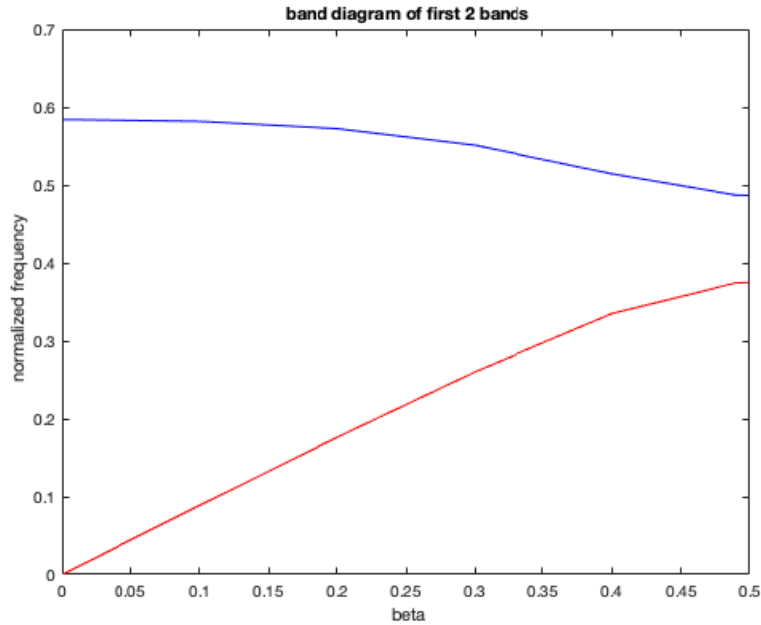
Figure 7. The band diagram for the two bands between Γ and X points for $\beta_2 = \beta_3 = 0$ and $0 \le \beta_1 \le \frac{\pi}{2}$.

Table 5. Eigen-frequency for X-point and Γ-point.

Location	β_1	1st band f_N	2nd band f_N
X point	0.5	0.3748	0.4867
Γ point	0	0	0.5839

9. CONCLUSIONS

In this paper, we apply the BBGF-KKR-MST method to calculate band eigenvalue frequencies, band fields, and the normalizations of band fields of scalar waves for 3D periodic structures. The advantages of the approach are (a) the dimension of the eigenvalue matrix equation is small which is only 4 by 4 for the first 2 bands, (b) the BBGF allows the calculation of the KKR matrix fast for many wavenumbers, and (c) the band field solutions are represented by 36 spherical wave coefficients.

In MST, the T matrix used is that of an isolated single scatterer which is independent of the lattice and independent of the Bloch vector. Thus, for a general scatterer, the T matrix can be precalculated separately using various techniques [49–52] such as MoM, FEM, and FDTD, and commercial software such as HFSS, FEKO, and CST in the frequency range of interest and then used for all lattices and Bloch vectors. This will further increase the computational efficiency of the BBGF-KKR-MST method. With the band field solutions determined, we will calculate the BBGF with the plurality of scatterers [53–56].

The transfer matrix of a scatterer is independent of the lattice. The Transfer T matrix is also independent of the Bloch vector $\bar{k}_i$. The calculation of T matrix for scatterer with an arbitrary shape is not difficult. The T matrix can be extracted from numerical software such as HFSS and FEKO. Recently we have used the method to extract the T matrix of a tree and also a plant. The shape of trees and plants are highly irregular. We have used the extracted T matrices with Foldy-Lax MST for scattering by a large number of trees/plants [52, 57]. The tree with primary and secondary braces is up to 40 wavelengths in height [57]. We will apply the same method of T matrix extraction to scatterers of arbitrary shape in photonic crystals.

For the case when the scatterer is dispersive with permittivity changing with frequency, the

technique can be extended readily to include T matrix for dispersive media. Such T matrix can be computed for spherical scatterers. The T matrix of arbitrary shaped scatterers can be extracted from commercial software [52, 57]. For the case when the background permittivity is dispersive, we will study the use of BBGF for efficient broadband computation of $\tilde{D}_{nm}(k, \bar{k}_i)$ coefficients.

In this paper we have studied the 3D scalar wave case. With appropriate T matrices, the scalar waves can be adapted to the case of acoustic waves [37] and electron waves. This paper initially formulates the eigen-value problem using integral equation (IE) which is lengthy. Based on the multiple scattering nature of periodical structure, Foldy Lax based formulation is then presented with the same final governing equation as IE's. Moreover, the formulation is much reduced. We have developed a fast computation method for the scalar 3D problem. Presently we are extending to vector 3D. When being completed, we will do a comparison with COMSOL with regard to accuracies and computation efficiency.

APPENDIX A.

In the literature and in open source codes [33, 45, 46], there are multiple definitions of associated Legendre polynomial and spherical harmonics. In Matlab there are built in functions for associated Legendre polynomials.

In this Appendix, we define the spherical harmonics and associated Legendre polynomial with superscript (N) to distinguish it from that in the book Tsang et al. Vol. 1 [33]. From [33], the associated Legendre polynomial is

$$P_n^m(x) = (-1)^m \left(1 - x^2\right)^{\frac{m}{2}} \frac{d^m}{dx^m} P_n(x) = \frac{(-1)^m}{2^n n!} \left(1 - x^2\right)^{\frac{m}{2}} \frac{d^{n+m}}{dx^{n+m}} \left(x^2 - 1\right)^n; \quad m = 0, \pm 1, ..., \pm n \quad \text{(A1)}$$

To relate between negative m and positive m,

$$P_n^{-m}(x) = (-1)^m \frac{(n-m)!}{(n+m)!} P_n^m(x) \tag{A2}$$

The spherical harmonic is

$$Y_n^m(\theta, \phi) = P_n^m(\cos\theta) e^{im\phi} \tag{A3}$$

The orthonormal relation is

$$\int_0^\pi d\theta \sin\theta \int_0^{2\pi} d\phi Y_n^m(\theta, \phi) Y_{n'}^{-m'}(\theta, \phi) = (-1)^m \frac{4\pi}{2n+1} \delta_{mm'} \delta_{nn'} \tag{A4}$$

The disadvantage of this definition is that the coefficients are small for negative m and large for positive m. We next define the (N) version

$$P_n^{(N)m}(x) = (-1)^m \sqrt{\frac{\left(n + \frac{1}{2}\right)(n-m)!}{(n+m)!}} P_n^m(x); \quad m = 0, \pm 1, ..., \pm n \tag{A5}$$

Then, relating negative m to positive m

$$P_n^{(N)(-m)}(x) = (-1)^m P_n^{(N)m}(x) \tag{A6}$$

In (N), the coefficient of positive m and negative m are of the same magnitude. spherical harmonics,

$$Y_n^{(N)m}(\theta, \phi) = \frac{1}{\sqrt{2\pi}} P_n^{(N)m}(\cos\theta) e^{im\phi} \tag{A7}$$

Changing to negative m,

$$Y_n^{(N)(-m)}(\theta, \phi) = (-1)^m \frac{1}{\sqrt{2\pi}} P_n^{(N)m}(\cos\theta) e^{-im\phi} \tag{A8}$$

For complex conjugate with superscript $*$

$$\left(Y_n^{(N)m}(\theta, \phi)\right)^* = \frac{1}{\sqrt{2\pi}} P_n^{(N)m}(\cos\theta) e^{-im\phi} \tag{A9}$$

The relation between negative m and complex conjugate is

$$Y_n^{(N)(-m)}(\theta, \phi) = (-1)^m \left(Y_n^{(N)m}(\theta, \phi)\right)^* \tag{A10}$$

The orthonormal relation for the integration of the product of spherical harmonic and complex conjugate is

$$\int_0^\pi d\theta \sin\theta \int_0^{2\pi} d\phi Y_n^{(N)m}(\theta, \phi) \left(Y_{n'}^{(N)m'}(\theta, \phi)\right)^* = \delta_{mm'}\delta_{nn'} \tag{A11}$$

The orthonormal relation for the integration of the product of two spherical harmonics is

$$\int_0^\pi d\theta \sin\theta \int_0^{2\pi} d\phi Y_n^{(N)m}(\theta, \phi) Y_{n'}^{(N)(-m')}(\theta, \phi) = (-1)^{m'} \delta_{mm'}\delta_{nn'} \tag{A12}$$

Using direction vector

$$\hat{r} = \sin\theta\cos\phi\hat{x} + \sin\theta\sin\phi\hat{y} + \cos\theta\hat{z} \tag{A13}$$

We can write

$$Y_n^{(N)m}(\theta, \phi) = Y_n^{(N)m}(\hat{r}) \tag{A14}$$

Reversing the direction means $(\theta, \phi) \rightarrow (\pi - \theta, \pi + \phi)$.

Then

$$P_n^{(N)m}(\cos(\pi - \theta)) = (-1)^{n+m} P_n^{(N)m}(\cos\theta) \tag{A15}$$

$$Y_n^{(N)m}(\pi - \theta, \pi + \phi) = Y_n^{(N)m}(-\hat{r}) = (-1)^n Y_n^{(N)m}(\hat{r}) = (-1)^n Y_n^{(N)m}(\theta, \phi) \tag{A16}$$

Computer codes for associated Legendre polynomials are built in functions of MATLAB. In using MATLAB, the readers need to check carefully the MATLAB definition of the associated Legendre polynomials.

APPENDIX B. COMPUTATIONS OF $P(L, L_1, L')$ AND $D_{LL_1}(K, \bar{K}_I)$

The definition is

$$P\left(l, l_1, l'\right) = P\left(n, m, n_1, m_1, n', m'\right) = (-1)^{n_1}(-1)^{m'+m_1} i^{n_1+n-n'}$$
$$\sqrt{(2n'+1)(2n_1+1)(2n+1)} \begin{pmatrix} n' & n_1 & n \\ 0 & 0 & 0 \end{pmatrix} \begin{pmatrix} n' & n_1 & n \\ -m' & -m_1 & m \end{pmatrix} \tag{B1}$$

The properties of Wigner 3j symbol $\begin{pmatrix} n' & n_1 & n \\ 0 & 0 & 0 \end{pmatrix}$ are [43]

$$|n - n_1| \leq n' \leq n + n_1 \tag{B2}$$

And

$$\begin{pmatrix} n' & n_1 & n \\ 0 & 0 & 0 \end{pmatrix} = 0 \quad \text{if } n' + n_1 + n \text{ is odd} \tag{B3}$$

This means $i^{n_1+n-n'} = i^{\text{even}}$, so that is $P(l, l_1, l')$ real.

In $\begin{pmatrix} n' & n_1 & n \\ -m' & -m_1 & m \end{pmatrix}$

$$-m' - m_1 + m = 0; \quad m' = m - m_1 \tag{B4}$$

Since

$$D_{ll_1}\left(k, \bar{k}_i\right) = \sum_{l'} P\left(l, l_1, l'\right) \tilde{D}_{l'}\left(k, \bar{k}_i\right) \tag{B5}$$

then

$$
\begin{aligned}
D_{ll_1}\left(k,\bar{k}_i\right) =\ & -\frac{h_0^{(1)}\left(kR\right)}{j_0\left(kR\right)}\sum_{l'} P\left(l,l_1,l'\right)\delta_{m'0}\delta_{n'0} + \frac{\sqrt{4\pi}}{ik}\sum_{l'} P\left(l,l_1,l'\right)\frac{I_1\left(n',m',i\xi,\bar{k}_i\right)}{j_{n'}\left(kR\right)} \\
& -\frac{\sqrt{4\pi}}{ik}\frac{\xi^2+k^2}{2\xi}\sum_{l'} P\left(l,l_1,l'\right)\frac{I_2\left(n',m',i\xi,\bar{k}_i\right)}{j_{n'}\left(kR\right)} \\
& +\frac{\sqrt{4\pi}}{ik}\frac{\left(\xi^2+k^2\right)^2}{8\xi}\sum_{l'} P\left(l,l_1,l'\right)\frac{I_3\left(n',m',i\xi,\bar{k}_i\right)}{j_{n'}\left(kR\right)} \\
& +\frac{\sqrt{4\pi}}{ik}\left(\xi^2+k^2\right)^3\sum_{l'} P\left(l,l_1,l'\right)\frac{1}{j_{n'}(kR)}\sum_{s} Q_{4n'}^{m'}(\bar{k}_{is})\frac{1}{\left(k_{is}^2-k^2\right)} \qquad (B6)
\end{aligned}
$$

In broadband computations of $D_{ll_1}(k,\bar{k}_i)$, terms that are independent of k are computed once. These include $P(l,l_1,l')$, $I_1(n',m',i\xi,\bar{k}_i)$, $I_2(n',m',i\xi,\bar{k}_i)$, $I_3(n',m',i\xi,\bar{k}_i)$, and $Q_{4n'}^{m'}(\bar{k}_{is})$.

Then for a given k, $D_{ll_1}(k,\bar{k}_i)$ are computed by putting in the simple k dependences. In this manner, $D_{ll_1}(k,\bar{k}_i)$ can be computed rapidly for many k's.

APPENDIX C. T MATRIX OF SCALAR WAVES

We consider the T matrix of scalar waves for a particle of radius b with wavenumber k_p in a background with wavenumber k.

For the exciting wave, the wave function is

$$
\psi_E = \sum_{n,m} a_{nm}^E Rg\psi_{nm}\left(k\bar{r}\right) \qquad (C1)
$$

The scattered wave is

$$
\psi_s = \sum_{n,m} a_{nm}^s \psi_{nm}\left(k\bar{r}\right) \qquad (C2)
$$

The field inside particle is

$$
\psi_p = \sum_{n,m} c_{nm} Rg\psi_{nm}\left(k_p\bar{r}\right) \qquad (C3)
$$

The boundary conditions are the continuity of wave functions and normal derivatives. Then the scattered wave coefficient is related to the exciting field coefficient by the T matrix coefficient T_n

$$
a_{nm}^s = T_n a_{nm}^E \qquad (C4)
$$

where the T matrix coefficient T_n is

$$
T_n = -\frac{kj_n'\left(ka\right)j_n\left(k_pa\right)-k_pj_n\left(ka\right)j_n'(k_pa)}{kh_n^{(1)'}\left(ka\right)j_n\left(k_pa\right)-k_ph_n^{(1)}\left(ka\right)j_n'(k_pa)} \qquad (C5)
$$

APPENDIX D. DERIVATION OF KKR BASED ON FOLDY-LAX (FL) MULTIPLE SCATTERING EQUATIONS

In the derivations of KKR equation, the common procedure is to use integral equations and the lattice Green's function. In this appendix, we give an alternative derivation based on Foldy-Lax (FL) Multiple Scattering equations without the use of integral equations. (Foldy 1945 [34]; Lax 1951 [35]; Tsang et al. 1982 [38]; Tsang et al. 1985 [39], Tsang et al., Vol. 2 [40]). The Foldy-Lax equations are usually used for random media with random positions of particles. However, it can be applied to periodic scatterers which is a special case of random media.

Consider N number of particles, centered at $\bar{R}_q$, $q = 1, 2, 3, ..., N$. The Foldy-Lax equations state that the exciting field of particle q, $\psi^{ex(q)}(\bar{r})$, is the incident wave, $a^{inc}(\bar{r})$, plus the scattered field from all particles p, $\psi^{s(p)}(\bar{r})$, except particle q itself (Tsang et al. 1985 [39]).

$$\psi^{ex(q)}(\bar{r}) = a^{inc}(\bar{r}) + \sum_{p \neq q}^{N} \psi^{s(p)}(\bar{r}) \tag{D1}$$

Note that the number of particles N can be infinite. The $\psi^{ex(q)}(\bar{r})$ is expanded in spherical waves centered at $\bar{R}_q$ and $\psi^{s(p)}(\bar{r})$ is expanded in spherical waves centered at $\bar{R}_p$

$$\psi^{ex(q)}(\bar{r}) = \sum_{n,m} \omega_{nm}^{(q)} Rg\psi\left(k\left(\bar{r} - \bar{R}_q\right)\right) \tag{D2}$$

$$\psi^{s(p)}(\bar{r}) = \sum_{n_1,m_1} a_{n_1 m_1}^{(s)(p)} \psi_{n_1 m_1}\left(k\left(\bar{r} - \bar{R}_p\right)\right) \tag{D3}$$

where $\omega_{nm}^{(q)}$ and $a_{n_1 m_1}^{(s)(p)}$ are exiting field coefficients of particle q and scattered field coefficients of particle p, respectively. We substitute (D2) and (D3) in (D1), and obtain (Tsang et al. 1982 [38], Tsang et al. 1985 [39], Tsang et al., Vol. 2 2001 [40]).

$$\sum_{n,m} \omega_{nm}^{(q)} Rg\psi\left(k\left(\bar{r} - \bar{R}_q\right)\right) = a^{inc}(\bar{r}) + \sum_{p \neq q}^{N} \sum_{n_1,m_1} a_{n_1 m_1}^{(s)(p)} \psi_{n_1 m_1}\left(k\left(\bar{r} - \bar{R}_p\right)\right) \tag{D4}$$

We next use the translation addition theorem for $r' > r''$. (Chew [45], page 593), taking into account the various definitions of associated Legendre polynomials and the spherical harmonics. We also make use of symmetry relations of Wigner 3j symbols (Edmonds [43]).

The translation theorem is

$$\psi_{n_1 m_1}\left(k\left(\bar{r}'' - \bar{r}'\right)\right) = \sqrt{4\pi} \sum_{n',m'} \sum_{n,m} \psi_{n'(-m')}\left(k\bar{r}'\right) Rg\psi_{nm}\left(k\bar{r}''\right) (-1)^{m'}$$
$$P\left(n, m, n_1, m_1, n', m'\right) \quad \text{for } r' > r'' \tag{D5}$$

where $P(n, m, n_1, m_1, n', m')$ is as defined in Equation (B1).

Since $\bar{r} - \bar{R}_p = \bar{r} - \bar{R}_q - (\bar{R}_p - \bar{R}_q)$, we let in (D5), $\bar{r}'' = \bar{r} - \bar{R}_q$ and $\bar{r}' = \bar{R}_p - \bar{R}_q$. Then

$$\psi_{n_1 m_1}\left(k(\bar{r} - \bar{R}_p)\right) = \sqrt{4\pi} \sum_{n',m'} \sum_{n,m} \psi_{n'(-m')}\left(k\left(\bar{R}_p - \bar{R}_q\right)\right) Rg\psi_{nm}\left(k\left(\bar{r} - \bar{R}_q\right)\right) (-1)^{m'}$$
$$P\left(n, m, n_1, m_1, n', m'\right) \quad \text{for } \left|\bar{R}_p - \bar{R}_q\right| > \left|\bar{r} - \bar{R}_q\right| \tag{D6}$$

Let the incident wave be expanded into spherical waves about $\bar{R}_q$.

$$a^{inc}(\bar{r}) = \sum_{n,m} a^{inc(q)} Rg\psi_{nm}\left(k\left(\bar{r} - \bar{R}_q\right)\right) \tag{D7}$$

Substitute (D6) and (D7) into (D4) and balance coefficients of the expansions $Rg\psi_{nm}(k(\bar{r} - \bar{R}_q))$.

$$\omega_{nm}^{(q)} = a^{inc(q)} + \sum_{p \neq q}^{N} \sum_{n_1,m_1} a_{n_1 m_1}^{(s)(p)} \sqrt{4\pi} \sum_{n',m'} \psi_{n'(-m')}\left(k\left(\bar{R}_p - \bar{R}_q\right)\right) (-1)^{m'} P\left(n, m, n_1, m_1, n', m'\right) \tag{D8}$$

The equation in (D8) of Foldy Lax in spherical wave expansions is applicable to both random and periodic systems. For periodic systems, we let the number of particles $N = \infty$.

Next we consider the periodic case of bands. Let there be no incident wave so that

$$a^{inc(q)} = 0 \tag{D9}$$

The Bloch condition relates scattered field and exciting field coefficients to the center cell $(0, 0, 0)$. This means

$$a_{n_1 m_1}^{(s)(p)} = a_{n_1 m_1}^{(s)} e^{i\bar{k}_i \cdot \bar{R}_p} \tag{D10}$$

$$\omega_{nm}^{(q)} = \omega_{nm} e^{i\bar{k}_i \cdot \bar{R}_q} \tag{D11}$$

where $a_{n_1 m_1}^{(s)}$ and ω_{nm} are the scattered field coefficients and exciting field coefficients in the center cell $(0, 0, 0)$. Then

$$\omega_{nm} = \sum_{n_1, m_1} a_{n_1 m_1}^{(s)} \sqrt{4\pi} \sum_{n', m'} (-1)^{m'} P\left(n, m, n_1, m_1, n', m'\right) \sum_{p \neq q} e^{i\bar{k}_i \cdot \left(\bar{R}_p - \bar{R}_q\right)} \psi_{n'(-m')}\left(k\left(\bar{R}_p - \bar{R}_q\right)\right) \tag{D12}$$

For periodic systems, the summation over particles p can be represented by

$$\sum_{p \neq q} e^{i\bar{k}_i \cdot \left(\bar{R}_p - \bar{R}_q\right)} \psi_{n'(-m')}\left(k\left(\bar{R}_p - \bar{R}_q\right)\right) = \sum_{s \neq (0,0,0)} e^{i\bar{k}_i \cdot \bar{R}_s} \psi_{n'(-m')}\left(k\bar{R}_s\right) \tag{D13}$$

Then

$$\omega_{nm} = \sum_{n_1, m_1} a_{n_1 m_1}^{(s)} \sqrt{4\pi} \sum_{n', m'} (-1)^{m'} P\left(n, m, n_1, m_1, n', m'\right) \sum_{s \neq (0,0,0)} e^{i\bar{k}_i \cdot \bar{R}_s} \psi_{n'(-m')}\left(k\bar{R}_s\right) \tag{D14}$$

Equation (D14) is the KKR equation with summation of spherical waves $\psi_{n'(-m')}(k\bar{R}_s)$ over all cells outside $(0, 0, 0)$ each weighted by $e^{i\bar{k}_i \cdot \bar{R}_s}$. We next make use of the $\tilde{D}_{nm}(k, \bar{k}_i)$ coefficients in (D14).

From Equations (10) and (16), the response Green's function $g_R(k, \bar{k}_i, \bar{r})$ is represented by summation over point sources from other cells weighted by the Bloch phase shift $e^{i\bar{k}_i \cdot \bar{R}_s}$. It is also given in terms of the $\tilde{D}_{nm}(k, \bar{k}_i)$ coefficients.

$$\begin{aligned} g_R\left(k, \bar{k}_i, \bar{r}\right) &= \sum_{s \neq (0,0,0)} e^{i\bar{k}_i \cdot \bar{R}_s} \frac{ik}{\sqrt{4\pi}} \psi_{00}\left(k\left(\bar{r} - \bar{R}_s\right)\right) \\ &= \sum_{s \neq (0,0,0)} e^{i\bar{k}_i \cdot \bar{R}_s} \frac{e^{ik|\bar{r} - \bar{R}_s|}}{4\pi |\bar{r} - \bar{R}_s|} \\ &= \frac{ik}{\sqrt{4\pi}} \sum_{n, m} \tilde{D}_{nm}\left(k, \bar{k}_i\right) Rg\psi_{nm}\left(k\bar{r}\right) \end{aligned} \tag{D15}$$

From Harrington (Time Harmonic Electromagnetic Fields) [58] and Sarabandi's book [59],

$$\frac{e^{ik|\bar{r} - \bar{R}_s|}}{4\pi |\bar{r} - \bar{R}_s|} = ik \sum_{n, m} (-1)^m \psi_{n(-m)}\left(k\bar{R}_s\right) Rg\psi_{nm}\left(k\bar{r}\right) \tag{D16}$$

Then substituting (D16) in (D15), we balance the coefficients of $Rg\psi_{nm}(k\bar{r})$.

$$\tilde{D}_{nm}\left(k, \bar{k}_i\right) = \sqrt{4\pi} (-1)^m \sum_{s \neq (0,0,0)} e^{i\bar{k}_i \cdot \bar{R}_s} \psi_{n(-m)}\left(k\bar{R}_s\right) \tag{D17}$$

We use (D17) to replace the $\sum_{s \neq (0,0,0)}$ equation in (D14).

The KKR equation becomes

$$\omega_{nm} = \sum_{n_1, m_1} a_{n_1 m_1}^{(s)} \sum_{n', m'} P\left(n, m, n_1, m_1, n', m'\right) \tilde{D}_{n'm'}\left(k, \bar{k}_i\right) \tag{D18}$$

The KKR Equation (D18) is identical to the KKR Equation (54) derived from integral equations.

REFERENCES

1. Wang, Z., Y. D. Chong, J. D. Joannopoulos, and M. Soljacic, "Reflection-free one-way edge modes in a gyromagnetic photonic crystal," *Phys. Rev. Lett.*, Vol. 100, 013905, 2008.
2. Yang, Z., F. Gao, X. Shi, X. Lin, Z. Gao, Y. Chong, and B. Zhang, "Topological acoustics," *Phys. Rev. Lett.*, Vol. 114, 114301, 2015.

3. Xue, H., Y. Yang, G. Liu, F. Gao, Y. Chong, and B. Zhang, "Realization of an acoustic third-order topological insulator," *Phys. Rev. Lett.*, Vol. 122, 244301, Jun. 2019.

4. Ao, X., Z. Lin, and C. T. Chan, "One way edge modes in a magneto-optical honeycomb photonic crystal," *Phys. Rev. B*, Vol. 80, 033105, 2009.

5. Tsaolamprou, A. C., M. Kafesaki, C. M. Soukoulis, E. N. Economou, and T. Koschny, "Chiral topological surface states on a finite square photonic crystal bounded by air," *Physical Review Applied*, Vol. 16, 044011, 2021

6. Zhao, R., G. D. Xie, M. L. N. Chen, Z. Lan, Z. Huang, and W. E. I. Sha, "First-principle calculation of Chern number in gyrotropic photonic crystals," *Optics Express*, Vol. 28, 4638, 2020.

7. Feng, Z., S. Tan, L. Tsang, and E. Li, "Band characterization of topological photonic crystals using the broadband Green's function technique," *Optics Express*, Vol. 28, No. 19, 27223, 2020.

8. Tsang, L., T.-H. Liao, and S. Tan, "Calculation of bands and band field solutions in topological acoustics using the broadband Green's function-KKR-multiple scattering method," *Progress In Electromagnetic Research*, Vol. 171, 137–158, 2021.

9. Ho, K. M., C. T. Chan, and C. M. Soukoulis, "Existence of a photonic gap in periodic dielectric structures," *Phys. Rev. Lett.*, Vol. 65, 3152–3155, 1990.

10. Leung, K. M. and Y. F. Liu, "Full vector wave calculation of photonic band structures in face-centered-cubic dielectric media," *Phys. Rev. Lett.*, Vol. 65, 2646–2649, 1990.

11. Plihal, M. and A. A. Maradudin, "Photonic band structure of two-dimensional systems: The triangular lattice," *Phys. Rev. B*, Vol. 44, 8565–8571, 1991.

12. Joannopoulos, J. D., S. G. Johnson, J. N. Winn, and R. D. Meade, *Photonic Crystals: Molding the Flow of Light*, Princeton University Press, 2011.

13. Nicolet, A., S. Guenneau, C. Geuzainec, and F. Zollaa, "Modelling of electromagnetic waves in periodic media with finite elements," *Journal of Comp. and Appl. Math.*, Vol. 168, 321–329, 2004.

14. Jin, J. M., *Finite Element Method in Electromagnetics*, 3rd Edition, Wiley, 2014.

15. Tsang, L., "Broadband calculations of band diagrams in periodic structures using the broadband Green's function with low wavenumber extraction (BBGFL)," *Progress In Electromagnetics Research*, Vol. 153, 57–68, 2015.

16. Tsang, L. and S. Tan, "Calculations of band diagrams and low frequency dispersion relations of 2D periodic dielectric scattering using broadband Green's function with low wavenumber extraction (BBGFL)," *Optics Express*, Vol. 24, 945–965, 2016.

17. Gao, R., L. Tsang, S. Tan, and T.-H. Liao, "Band calculations using broadband Green's functions and the KKR method with applications to magneto-optics and photonic crystals," *Journal of Optical Society of America B*, Vol. 37, 3896–3907, 2020.

18. Gao, R., L. Tsang, S. Tan, and T.-H. Liao, "Broadband Green's function-KKR-multiple scattering method for calculations of normalized band field solutions in magnetic-optics crystals," *Journal of Optical Society of America B*, Vol. 38, 3159–3171, 2021.

19. Tan, S. and L. Tsang, "Efficient broadband evaluations of lattice Green's functions via imaginary wavenumber components extractions," *Progress In Electromagnetics Research*, Vol. 164, 63–74, 2019.

20. Sanamzadeh, M. and L. Tsang, "Fast and broad band calculation of the dyadic Green's function in the rectangular cavity; An imaginary wave number extraction technique," *Progress In Electromagnetic Research C*, Vol. 96, 243–258, 2019.

21. Liao, T.-H., L. Tsang, and W. Kwek, "Broadband Green's Funtion (BBGFL) method with imaginary wavenumber extractions for simulations of radiated emissions from irregular shaped printed circuit board," *IEEE Transactions on Electromagnetic Compatibility*, Vol. 62, No. 5, 2209–2216, Oct. 2020.

22. Korringa, J., "On the calculation of the energy of a Bloch wave in a metal," *Physica*, Vol. 13, 392–400, 1947.

23. Kohn, W. and N. Rostoker, "Solution of the Schrodinger equation in periodic lattices with an application to metallic lithium," *Phys. Rev.*, Vol. 94, 1111–1120, 1954.

24. Ham, F. S. and B. Segall, "Energy bands in periodic lattices — Green's function method," *Phys. Rev.*, Vol. 124, No. 6, 1786–1796, 1961.

25. Wang, X., X. G. Zhang, Q. Yu, and B. N. Harmon, "Multiple scattering theory for electromagnetic waves," *Phys. Rev. B*, Vol. 47, No. 8, 4161–4167, 1993.

26. Leung, K. M. and Y. Qiu, "Multiple-scattering calculation of the two-dimensional photonic band structure," *Phys. Rev. B*, Vol. 48, 7767–7771, 1993.

27. Kafesaki, M. and F. Economou, "Multiple-scattering theory for three-dimensional periodic acoustic composites," *Phys. Rev. B*, Vol. 60, 11993–12001, 1999.

28. Liu, Z., C. T. Chan, P. Sheng, A. L. Goertzen, and J. H. Page, "Elastic wave scattering by periodic structures of spherical objects: Theory and experiment," *Phys. Rev. B*, Vol. 62, 2446–2457, 2000.

29. Kambe, K., "Theory of low-energy electron diffraction," *I. Application of the Cellular Method to Monatomic Layers*, Vol. 22, No. 3, 322–330, 1967.

30. Kambe, K., "Theory of electron diffraction by crystals," *I. Green's Function and Integral Equation*, Vol. 22, No. 4, 422–431, 1967.

31. Kambe, K., "Theory of low-energy electron diffraction," *II. Cellular Method for Complex Monolayers and Multilayers*, Vol. 23, No. 9, 1280–1294, 1968.

32. Jia, P.-H., et al., "Two fold domain decomposition method for the analysis of multiscale composite structures," *IEEE Transactions on Antennas and Propagation*, Vol. 67, No. 9, 6090–6103, Sep. 2019.

33. Tsang, L., J. A. Kong, and K. H. Ding, *Scattering of Electromagnetic Waves, Vol. 1: Theory and Applications*, 426 pages, Wiley Interscience, 2000.

34. Foldy, L. L., "The multiple scattering of waves. I. General theory of isotropic scattering by randomly distributed scatterers," *Phys. Rev.*, Vol. 67, 107–119, 1945.

35. Lax, M., "Multiple scattering of waves," *Rev. Mod. Phys.*, Vol. 23, No. 4, 287–310, 1951.

36. Waterman, P. C. and R. Truell, "Multiple scattering of waves," *Journal of Mathematical Physics*, Vol. 2, No. 4, 512–537, 1961.

37. Ishimaru, A., *Wave Propagation and Scattering in Random Media*, Academic Press, 1978.

38. Tsang, L., J. A. Kong, and T. Habashy, "Multiple scattering of acoustic waves by random distribution of discrete spherical scatterers with the quasicrystalline and Percus-Yevick approximation," *Journal of the Acoustical Society of America*, Vol. 71, No. 3, 552–558, Mar. 1982.

39. Tsang, L., J. A. Kong, and R. Shin, *Theory of Microwave Remote Sensing*, Wiley-Interscience, New York, 1985.

40. Tsang, L., J. A. Kong, K. H. Ding, and C. O. Ao, *Scattering of Electromagnetic Waves, Vol. 2: Numerical Simulations*, 705 pages, Wiley Interscience, 2001.

41. Mishchenko, M. I., L. D. Travis, and A. A. Laci's, *Multiple Scattering of Light by Particles, Radiative Transfer and Coherent Backscattering*, Cambridge University Press, 2006.

42. Stein, S., "Addition theorem for spherical wave functions," *Quarterly of Applied Mathematics*, Vol. 19, No. 1, 15–24, 1961.

43. Edmonds, A. R., *Angular Momentum in Quantum Mechanics*, Princeton University Press, 1960.

44. Cruzan, O. R., "Translational addition theorem for spherical vector wave functions," *Q. Appl. Math*, Vol. 20, 33–40, 1962.

45. Chew, W. C., *Waves and Fields in Inhomogeneous Media*, IEEE Press, 1995.

46. Abramowitz, M. and I. Stegun, *Handbook of Mathematical Functions*, Dover, 1956.

47. Waterman, P. C., "Matrix formulation of electromagnetic scattering," *Proceedings of IEEE*, Vol. 53, 805–812, 1965.

48. Gradshteyn, I. S. and I. M. Ryzhik, *Table of Integrals, Series, and Products*, Academic Press, 2007.

49. Huang, H., L. Tsang, A. Colliander, R. Shah, X. Xu, and S. H. Yueh, "Multiple scattering of waves by complex objects using hybrid method of T-matrix and foldy-lax equations using vector spherical waves and vector spheroidal waves," *Progress In Electromagnetic Research*, Vol. 168, 87–111, 2020.

50. Gu, W., L. Tsang, A. Colliander, and S. Yueh, "Propagation of waves in vegetations using a hybrid method," *IEEE Transactions on Antennas and Propagation*, Vol. 69, No. 10, 6752–6761, Oct. 2021.

51. Gu, W., L. Tsang, A. Colliander, and S. Yueh, "Multifrequency full-wave simulations of vegetation using a hybrid method," *IEEE Transactions on Microwave Theory and Techniques*, Vol. 70, No. 1, 275–285, Jan. 2022.

52. Tsang, L., T.-H. Liao, R. Gao, H. Xu, W. Gu, and J. Zhu, "Theory of microwave remote sensing of vegetation effects, soop and rough soil surface backscattering," *Remote Sensing*, Vol. 14, No. 15, 2022.

53. Tan, S. and L. Tsang, "Green functions, including scatterers, for photonic crystals and metamaterials," *Journal of Optical Society of America B*, Vol. 34, 1450–1458, 2017.

54. Tan, S. and L. Tsang, "Scattering of waves by a half-space of periodic scatterers using broadband Green's function," *Opt. Lett.*, Vol. 42, No. 22, 4667–4670, Nov. 2017.

55. Tsang, L., K.-H. Ding, and S. Tan, "Broadband point source Green's function in a one-dimensional infinite periodic lossless medium based on BBGFL with modal method," *Progress In Electromagnetics Research*, Vol. 163, 51–77, 2018.

56. Tsang, L. and S. Tan, "Full wave simulations of photonic crystals and metamaterials using the broadband Green's functions," US patent number 11,087,043, Aug. 10, 2021.

57. Gu, W., L. Tsang, A. Colliander, and S. Yueh, "Hybrid method for full-wave simulations of forests at L-band," *IEEE Access*, Vol. 10, 105898–105909, 2022.

58. Harrington, R. F., *Time-harmonic Electromagnetic Fields*, McGraw-Hill, 1961.

59. Sarabandi, K., *Foundations of Applied Electromagnetics*, Michigan Publishing, 2022.